Since we found that the preparation of sufficiently active $TrClO_4$ was not always reproducible, we compared several sources of Tr^+ and chose trityl *N,N*-bis(trifluoromethanesulfonic)imidate (TrNTf_2), which was superior in terms of preparation, handling, and reactivity to the others ($TrClO_4$, $TrOCOCF_3$, TrOTf, and $TrPF_6$). First of all, glycosylation of cholesterol **2**[9] was chosen as a model reaction and the reactions were carried out with donor **1** (3.0 equiv) and cholesterol **2** (1.0 equiv) in the presence of $TrNTf_2$ (6.0 equiv) in pure or mixed solvents at 0 °C for optimization of the reaction conditions (Table 1). CH_2Cl_2 was used as a solvent in every case to dissolve highly lipophilic cholesterol **2**, and toluene, MeCN, dioxane, and THF were tested as cosolvents. We found that the yield of the desired product **3** was low when the reaction was conducted in CH_2Cl_2 (entry 1) and the addition of nonpolar toluene did not improve the result (entry 2). In contrast, the use of polar MeCN and 1,4-dioxane as cosolvents improved the yield (entries 1 vs 3 and 4) and 1,4-dioxane with a little higher Gutmann donor number (DN)[10] (14.8) than MeCN (14.1) gave a better result. However, the use of THF as a cosolvent resulted in a poor yield of **3** (entry 5), which can probably be attributed to the deactivation of $TrNTf_2$ by highly coordinating THF (DN = 20.0); the color of the reaction mixture gradually changed from clear yellow to black.[11] The modest Lewis basicity of dioxane may be appropriate to promote this reaction without deactivating $TrNTf_2$. Thus, the desired product **3** was obtained in a modest yield via the novel Tr^+-promoted glycosylation. But the yield was not improved further by changing reaction conditions. For example, reactions conducted at rt yielded substantial byproducts. The main byproduct was 1-deoxy-2,3,4,6-tetra-*O*-Bn-glucose, which was probably formed by the reduction of the oxocarbenium ion generated from **1** with the BH_3 group of another molecule of **1**. Lowering the temperature significantly slowed down the reaction and the desired product **3** was not obtained in sufficient yield even with extended reaction time (entry 6).

In order to improve the reaction, we next focused on the use of trityl ethers as glycosyl acceptors. Thus, *O*-tritylcholesterol **5**[12] was used in the place of cholesterol **2** and detritylated in situ by TfOH.

Table 1
Tr^+-promoted glycosylation of cholesterol **2** with glycosyl boranophosphotriester derivative **1**

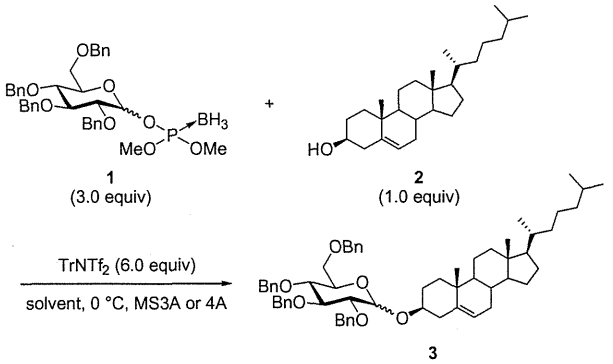

Entry	Solvent	Time (min)	Yield (%)[a] (α:β)[b]
1	CH_2Cl_2	40	21 (34:66)
2	Toluene–CH_2Cl_2 (2:1, v/v)	30	22 (52:48)
3	MeCN–CH_2Cl_2 (4:1, v/v)	30	35 (17:83)
4	Dioxane–CH_2Cl_2 (2:1, v/v)	40	60 (38:62)
5[c]	THF–CH_2Cl_2 (4:3, v/v)	60	22 (46:54)
6[d]	Dioxane–CH_2Cl_2 (1:1, v/v)	120	33 (32:68)

[a] Isolated yield.
[b] Determined by ^1H NMR.
[c] Additional 8.0 equiv of $TrNTf_2$ was added after 40 min.
[d] Reaction was conducted at −20 °C.

Table 2
Glycosylation using *O*-tritylcholesterol **5** as acceptor

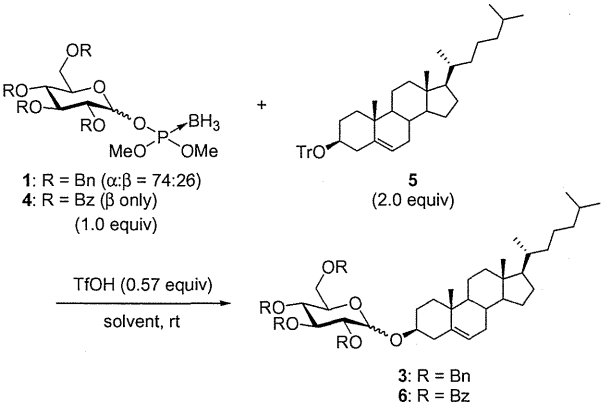

Entry	Donor	Solvent	Time (min)	Yield (%)[a] (α:β)[b]
1	**1**	CH_2Cl_2	240	40 (54:46)
2	**1**	Dioxane–CH_2Cl_2 (2:1, v/v)	10	76 (77:23)
3	**1**	Dioxane	10	83 (83:17)
4	**4**	CH_2Cl_2	120	61 (β Only)
5	**4**	Dioxane–CH_2Cl_2 (2:1, v/v)	10	74 (β Only)
6	**4**	dioxane	10	67 (β Only)
7[c]	**1**	Dioxane–CH_2Cl_2 (2:1, v/v)	30	55 (74:26)

[a] Isolated yield.
[b] Determined by ^1H NMR.
[c] 2.0 equiv of $TrNTf_2$ and 2.0 equiv of cholesterol were used as activator and acceptor, respectively.

The resultant Tr^+ would activate the glycosyl boranophosphotriesters to promote the glycosylation of cholesterol generated from **5** in situ. As reported in the literature,[13] the use of *O*-tritylalcohols as glycosyl acceptors in the place of alcohols is advantageous when complex acceptors are used because protecting group-manipulation is simplified and this would also allow us to circumvent the use of moisture-sensitive $TrNTf_2$.

As shown in Table 2, per-*O*-Bn- and Bz-glycosyl boranophosphotriesters (**1** and **4**) were allowed to react with *O*-tritylcholesterol **5** in the presence of TfOH in CH_2Cl_2, dioxane, or a 1:2 mixture of these two solvents. Tf_2NH was found to be ineffective probably because of the low solubility in CH_2Cl_2. Compared with the method using $TrNTf_2$ and cholesterol **2**, the desired product **3** was obtained in better yield (entries 2 vs 7). Per-*O*-Bn-donor **1** gave the product **3** as an α,β-mixture, while the per-*O*-Bz counterpart **4** gave β-**6** stereoselectively, indicating that the reaction proceeded via the

Table 3
Optimization of molar equivalent of trityl ether **5**[a]

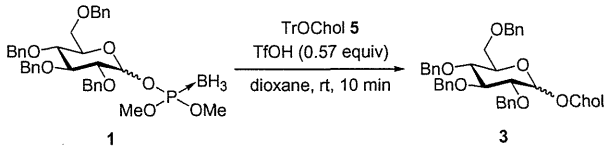

Entry	equiv of **5**	Yield (%)[b]	α:β[c]
1	1.2	34	80:20
2	1.5	45	87:13
3	2.0	83	83:17

[a] Chol = cholesteryl.
[b] Isolated yield.
[c] Determined by ^1H NMR.

Please cite this article in press as: Tatsumi, S.; et al. *Tetrahedron Lett.* (2013), http://dx.doi.org/10.1016/j.tetlet.2013.04.032

Table 4
Glycosylations using glycosyl boranophosphotriesters as glycosyl donors and *O*-tritylalcohols as glycosyl acceptors

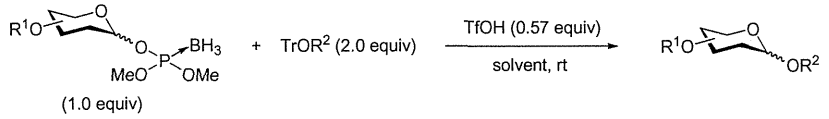

Entry	Donor (α:β)[b]	Acceptor	Solvent	Time (min)	Product	Yield (%)[a] (α:β)[b]
1	**1** (74:26)	**5**	Dioxane	10	**3**	83 (83:17)
2	**7** (67:33)	**5**	Dioxane	10	**12**	74 (67:33)
3	**8** (90:10)	**5**	Dioxane	10	**13**	71 (69:31)
4	**1** (74:26)	**11**	Dioxane	10	**14**	68 (83:17)
5	**7** (67:33)	**11**	Dioxane	10	**15**	56 (79:21)
6	**8** (90:10)	**11**	Dioxane	15	**16**	64 (63:37)
7	**4** (4:96)	**5**	Dioxane–CH_2Cl_2 (2:1, v/v)	10	**6**	74 (β Only)
8	**9** (7:93)	**5**	Dioxane–CH_2Cl_2 (2:1, v/v)	10	**17**	83 (β Only)
9	**10** (96:4)	**5**	Dioxane–CH_2Cl_2 (2:1, v/v)	10	**18**	77 (α Only)
10	**4** (4:96)	**11**	Dioxane–CH_2Cl_2 (2:1, v/v)	15	**19**	72 (β Only)
11	**9** (7:93)	**11**	Dioxane–CH_2Cl_2 (2:1, v/v)	15	**20**	77 (β Only)
12	**10** (96:4)	**11**	Dioxane–CH_2Cl_2 (2:1, v/v)	15	**21**	73 (α Only)

[a] Isolated yield.
[b] Determined by ^1H NMR.

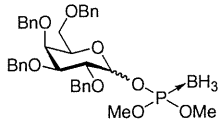

7

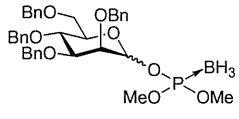

8

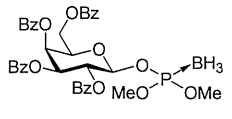

9

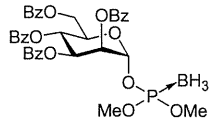

10

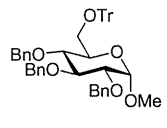

11

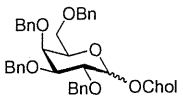

12

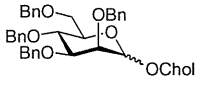

13

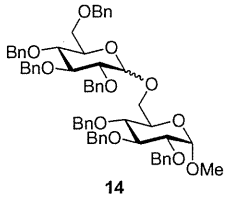

14

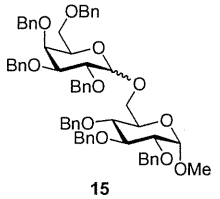

15

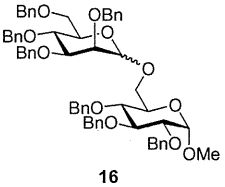

16

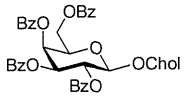

17

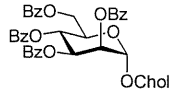

18

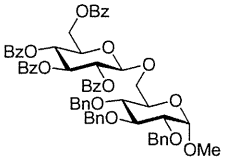

19

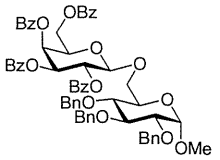

20

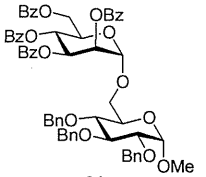

21

oxocarbenium ions and the 1,2-*trans*-selectivity of **6** was due to the neighboring group participation. Notably, the reaction rate was dramatically increased when dioxane was used as a (co)solvent (entries 1 vs 2, 3 and 4 vs 5, 6). It is also notable that the generation of Ph_3CH was confirmed by ^1H NMR analysis of the crude mixtures, indicating that the glycosyl donors **1** and **4** were oxidatively activated by Tr^+ derived from **5**.

Next, we conducted the reaction between **1** and **5** with different molar ratios (Table 3). 1.2, 1.5, or 2.0 equiv of the trityl ether **5** was used and found that the reaction was accomplished when 2.0 equiv of **5** was used (analyzed by TLC). Thus we used 2.0 equiv of trityl ethers as glycosyl acceptors in the following study.

By using the optimized conditions, glycosylation reactions using six kinds of per-*O*-Bn and Bz-glycosyl boranophosphotriesters (**1**, **4**, and **7**–**10**) were carried out (Table 4). The O^6-tritylglucoside derivative **11**[14] was employed as a glycosyl acceptor in addition to *O*-tritylcholesterol **5**. All the reactions were completed within 10–15 min and the desired products were obtained in moderate to good yields. Per-*O*-Bn-donors **1**, **7**, and **8** gave the products **3** and **12**–**16** as α,β-mixtures (entries 1–6), while the per-*O*-Bz counterparts (**4**, **9** and **10**) afforded the products (**6** and **17**–**21**) with complete 1,2-*trans*-selectivity (entries 7–12).

In conclusion, we developed a novel glycosylation that uses glycosyl boranophosphotriesters as glycosyl donors. Two types of reactions were studied, that is, (1) the donor was activated with $TrNTf_2$ to react with an alcohol and (2) *O*-trityl ethers worked as both glycosyl acceptors and Tr^+ sources. The latter was found to give better results and the desired *O*-glycosylation products were rapidly generated and isolated in moderate to good yields. Further study on the reaction mechanism as well as the application of this new glycosylation to the synthesis of more complex molecules is now in progress.

Acknowledgments

We thank Professor Kazuhiko Saigo (Kochi University of Technology) for helpful suggestions. This work was financially supported by the Ministry of Education, Culture, Sports, Science, and Technology (MEXT) Japan.

Please cite this article in press as: Tatsumi, S.; et al. *Tetrahedron Lett.* (2013), http://dx.doi.org/10.1016/j.tetlet.2013.04.032

Supplementary data

Supplementary data (experimental details) associated with this article can be found, in the online version, at http://dx.doi.org/10.1016/j.tetlet.2013.04.032.

References and notes

1. For reviews, see: (a) Palmacci, E. R.; Plante, O. J.; Seeberger, P. H. *Eur. J. Org. Chem.* **2002**, 595–606; (b) Vankayalapati, H.; Jiang, S.; Singh, G. *Synlett* **2002**, 16–25; (c) Oka, N.; Sato, K.; Wada, T. *Trends Glycosci. Glycotechnol.* **2012**, *24*, 152–168.
2. (a) Hashimoto, S.; Honda, T.; Ikegami, S. *J. Chem. Soc., Chem. Commun.* **1989**, 685–687; (b) Plante, O. J.; Andrade, R. B.; Seeberger, P. H. *Org. Lett.* **1999**, *1*, 211–214.
3. (a) Michalska, M.; Borowiecka, J. *J. Carbohydr. Chem.* **1983**, *2*, 99–103; (b) Inazu, T.; Hosokawa, H.; Satoh, Y. *Chem. Lett.* **1985**, 297–300; (c) Michalska, M.; Michalski, J. *Heterocycles* **1989**, *28*, 1249–1256; (d) Hashimoto, S.; Honda, T.; Ikegami, S. *Tetrahedron Lett.* **1990**, *31*, 4769–4772; (e) Hashimoto, S.; Honda, T.; Ikegami, S. *Tetrahedron Lett.* **1991**, *32*, 1653–1654; (f) Yamanoi, T.; Nakamura, K.; Sada, S.; Goto, M.; Furusawa, Y.; Takano, M.; Fujioka, A.; Yanagihara, K.; Satoh, Y.; Hosokawa, H.; Inazu, T. *Bull. Chem. Soc. Jpn.* **1993**, *66*, 2617–2622; (g) Plante, O. J.; Seeberger, P. H. *J. Org. Chem.* **1998**, *63*, 9150–9151.
4. (a) Hashimoto, S.; Sakamoto, H.; Honda, T.; Ikegami, S. *Tetrahedron Lett.* **1997**, *38*, 5181–5184; (b) Hashimoto, S.; Sakamoto, H.; Honda, T.; Abe, H.; Nakamura, S.; Ikegami, S. *Tetrahedron Lett.* **1997**, *38*, 8969–8972; (c) Sakamoto, H.; Nakamura, S.; Tsuda, T.; Hashimoto, S. *Tetrahedron Lett.* **2000**, *41*, 7691–7695; (d) Plante, O. J.; Palmacci, E. R.; Andrade, R. B.; Seeberger, P. H. *J. Am. Chem. Soc.* **2001**, *123*, 9545–9554.
5. For a review, see: Demchenko, A. V. *Lett. Org. Chem.* **2005**, *2*, 580–589.
6. (a) Ross, A. J.; Higson, A. P.; Ferguson, M. A. J.; Nikolaev, A. V. *Tetrahedron Lett.* **1999**, *40*, 6695–6698; (b) Prosperi, D.; Panza, L.; Poletti, L.; Lay, L. *Tetrahedron* **2000**, *56*, 4811–4815; (c) Routier, F. H.; Higson, A. P.; Ivanova, I. A.; Ross, A. J.; Tsvetkov, Y. E.; Yashunsky, D. V.; Bates, P. A.; Nikolaev, A. V.; Ferguson, M. A. J. *Biochemistry* **2000**, *39*, 8017–8025.
7. (a) Matsumura, F.; Oka, N.; Wada, T. *Org. Lett.* **2008**, *10*, 1557–1560; (b) Matsumura, F.; Oka, N.; Wada, T. *Org. Lett.* **2008**, *10*, 5297–5300; (c) Sato, K.; Oka, N.; Fujita, S.; Matsumura, F.; Wada, T. *J. Org. Chem.* **2010**, *75*, 2147–2156; (d) Fujita, S.; Oka, N.; Matsumura, F.; Wada, T. *J. Org. Chem.* **2011**, *76*, 2648–2659.
8. Li, P.; Sergueeva, Z. A.; Dobrikov, M.; Shaw, B. R. *Chem. Rev.* **2007**, *107*, 4746–4796.
9. (a) Shingu, Y.; Nishida, Y.; Dohi, H.; Kobayashi, K. *Org. Biol. Chem.* **2003**, *1*, 2518–2521; (b) Wunder, C.; Churin, Y.; Winau, F.; Warnecke, D.; Vieth, M.; Lindner, B.; Zähringer, U.; Mollenkopf, H.-J.; Heinz, E.; Meyer, T. F. *Nat. Med.* **2006**, *12*, 1030–1037.
10. Gutmann, V. *The Donor–Acceptor Approach to Molecular Interactions*; Plenum Press: New York, 1978.
11. Dreyfuss, M. P.; Westfahl, J. C.; Dreyfuss, P. *Macromolecules* **1968**, *1*, 437–441.
12. Colin-Messager, S.; Girard, J.-P.; Rossi, J.-C. *Tetrahedron Lett.* **1992**, *33*, 2689–2692.
13. (a) Betaneli, V. I.; Ovchinnikov, M. V.; Backinowsky, L. V.; Kochetkov, N. K. *Carbohydr. Res.* **1979**, *76*, 252–256; (b) Kochetkov, N. K.; Klimov, E. M.; Malysheva, N. N.; Demchenko, A. V. *Carbohydr. Res.* **1991**, *212*, 77–91; (c) Boons, G.-J.; Bowers, S.; Coe, D. M. *Tetrahedron Lett.* **1997**, *38*, 3773–3776.
14. Gollner, C.; Philipp, C.; Dobner, B.; Sippl, W.; Schmidt, M. *Carbohydr. Res.* **2009**, *344*, 1628–1631.

Please cite this article in press as: Tatsumi, S.; et al. *Tetrahedron Lett.* (2013), http://dx.doi.org/10.1016/j.tetlet.2013.04.032

Journal of Fluorine Chemistry 150 (2013) 85–91

Contents lists available at SciVerse ScienceDirect

Journal of Fluorine Chemistry

journal homepage: www.elsevier.com/locate/fluor

Short communication

Stereocontrolled synthesis of dinucleoside phosphorothioates using a fluorous tag

Natsuhisa Oka, Ryosuke Murakami, Tomoaki Kondo, Takeshi Wada *

Department of Medical Genome Sciences, Graduate School of Frontier Sciences, The University of Tokyo, Bioscience Building 702, 5-1-5 Kashiwanoha, Kashiwa, Chiba 277-8562, Japan

ARTICLE INFO

Article history:
Received 23 February 2013
Received in revised form 15 March 2013
Accepted 15 March 2013
Available online 26 March 2013

Keywords:
Stereocontrolled synthesis
Phosphorothioate
Fluorous
Oxazaphospholidine

ABSTRACT

Dinucleoside phosphorothioates were synthesized in a stereocontrolled manner (diastereoselectivity > 99:1) by using thymidine derivatives bearing a simple perfluoroalkyl tag (C_6F_{13} or C_8F_{17}) at the 3′-end and diastereopure nucleoside 3′-*O*-oxazaphospholidine monomers. Fluorous-tagged intermediates in the synthesis were easily purified by a simple fluorous solid-phase extraction process.

1. Introduction

Chemically modified oligonucleotides have found a wide range of applications, such as therapeutics, diagnostics, and nanotechnology [1–4]. In particular, their therapeutic applications have received renewed interest due to some newly discovered gene silencing processes, such as RNA interference, in which relatively short oligonucleotides regulate gene expression in a sequence-specific manner [5–7]. Many kinds of chemically modified oligonucleotides have been developed for these applications and the methods for their synthesis have also been continuously studied [1]. We have also developed a method to synthesize backbone-modified oligonucleotide analogs [8], such as phosphorothioates [9] and boranophosphates [10], in a stereocontrolled manner by using diastereopure nucleoside 3′-*O*-oxazaphospholidine derivatives [11] as monomer units, because the properties of these oligonucleotide analogs as drugs can be significantly affected by the configuration of phosphorus atoms [8f–i,9c,d].

One of the problems of these methods including ours is how to scale up the synthesis. Because these methods use reactions between oligonucleotides on insoluble solid-supports and reagents in solution-phase, large excess amounts of reagents are generally required to complete the reactions, and thus direct application of these methods to a large scale synthesis would be problematic.

To overcome this problem, we turned our attention to fluorous chemistry [12]. In contrast to the solid-phase synthesis, the fluorous chemistry consists of reactions in homogeneous media with stoichiometric amounts of reagents and facile purifications of the synthetic intermediates by liquid–liquid [12b] or solid–liquid extraction [12d] procedures utilizing the affinity of fluorous tags or supports [12b], which are attached to the intermediates, to fluorous solvents or silica gel. Fluorous chemistry has already been applied to the synthesis of oligopeptides and oligosaccharides [13,14], whereas its applications to the synthesis of oligonucleotides are scarce. To date, the only application is a fluorous-tagging of oligonucleotides, which are synthesized on insoluble solid-supports, while syntheses of oligonucleotides on fluorous supports have not been reported [15]. Under these circumstances, we have started to explore the applicability of the fluorous chemistry to a large-scale synthesis of stereoregulated oligonucleoside phosphorothioates. In this paper, we describe the preliminary results of this study.

2. Results and discussion

First, we attempted to tag the 3′-end of 5′-*O*-(4,4′-dimethoxytrityl)thymidine [5′-*O*-(DMTr)thymidine] **1** with an acyl chloride bearing a C_8F_{17} group (**2**) (Scheme 1). However, although the fluorous-tagged thymidine derivative **3** was generated smoothly, the product **3** turned out to be sparingly soluble in common organic solvents. Because the poor solubility of **3** in organic solvents would hamper the following synthesis of

* Corresponding author. Tel.: +81 4 7136 3611.
E-mail address: wada@k.u-tokyo.ac.jp (T. Wada).

0022-1139/$ – see front matter © 2013 Elsevier B.V. All rights reserved.
http://dx.doi.org/10.1016/j.jfluchem.2013.03.013

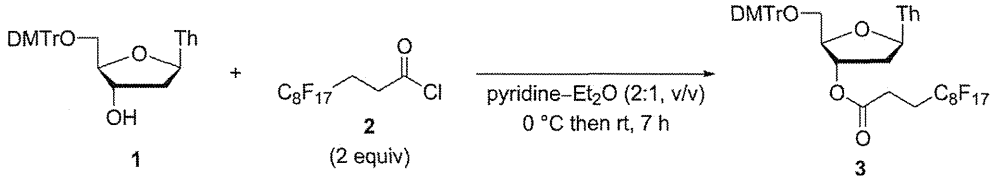

Scheme 1. Synthesis of 3′-fluorous-tagged thymidine derivative **3**. Th = thymin-1-yl.

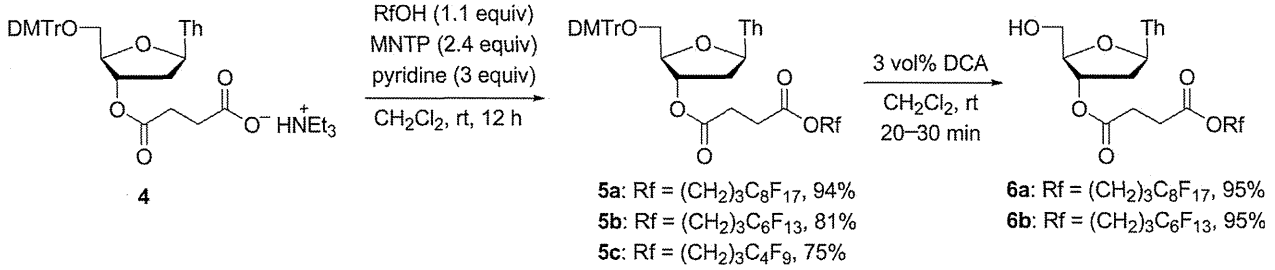

Scheme 2. 3′-Fluorous-tagging of thymidine derivative via succinate linker.

oligonucleotides, we inserted a succinate linker between the thymidine derivative and a fluorous tag so that the resultant fluorous-tagged thymidine would be sufficiently soluble in organic solvents. As shown in Scheme 2, a 5′-O-(DMTr)thymidine derivative bearing a succinate linker at the 3′-position (**4**) was condensed with commercially available 3-(perfluoroalkyl)propanols in the presence of 1,3-dimethyl-2-(3-nitro-1,2,4-triazol-1-yl)-2-pyrrolidin-1-yl-1,3,2-diazaphospholidinium hexafluorophosphate (MNTP) [16] as a condensing agent. Three kinds of 3-(perfluoroalkyl)propanols (perfluoroalkyl = C_8F_{17}, C_6F_{13}, C_4F_9) were employed as fluorous tags. The resultant fluorous-tagged thymidine derivatives **5a–c** were soluble in common organic solvents, such as dichloromethane, and were purified by a regular silica gel column chromatography.

Next, we investigated the affinity of **5a–c** to fluorous silica gel by using a regular fluorous solid-phase extraction (FSPE) process

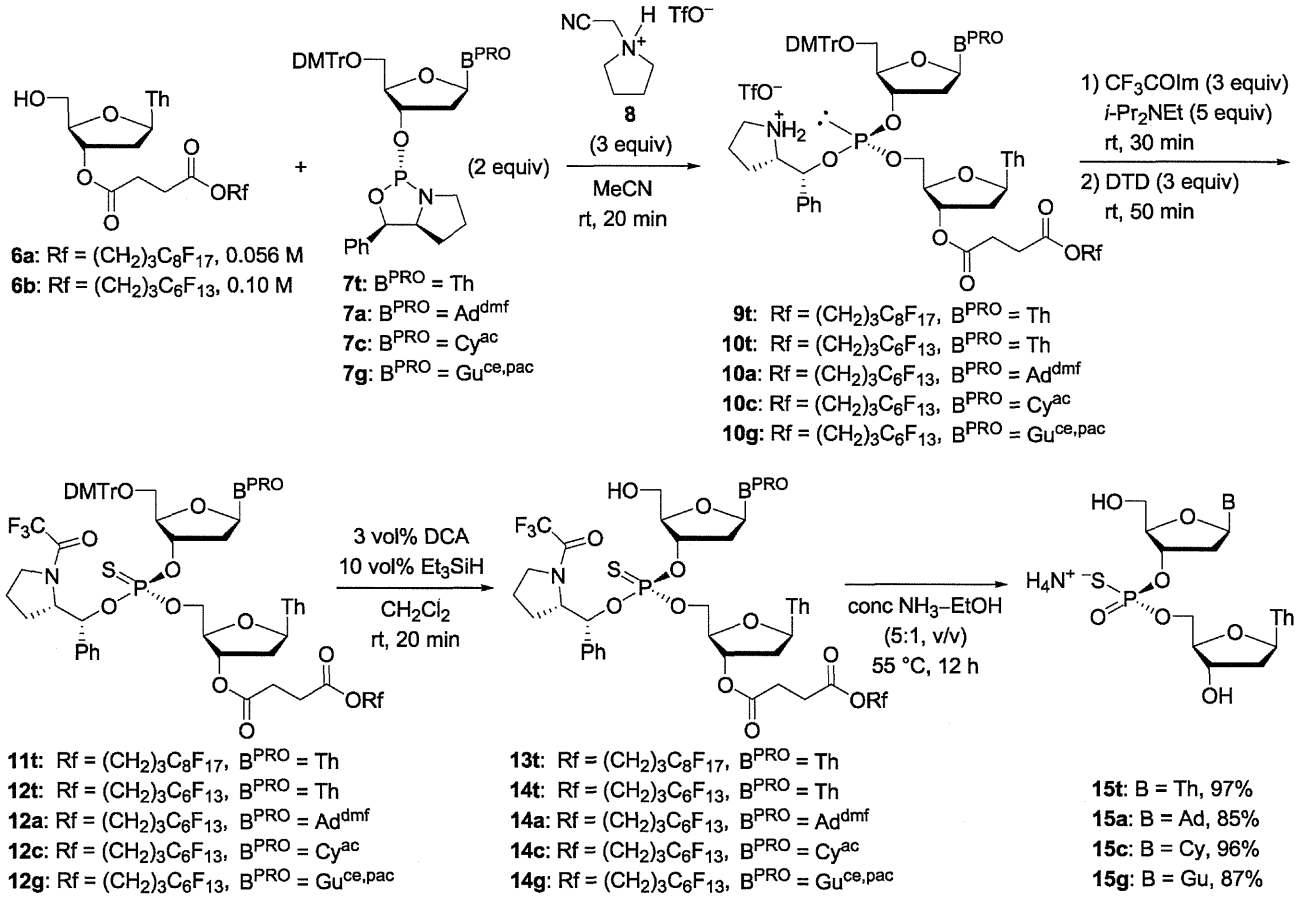

Scheme 3. Stereocontrolled synthesis of dinucleoside phosphorothioates **15t,a,c,g** using fluorous tags. B^{PRO} = protected nucleobase; Cy^{ac} = N^4-acetylcytosin-1-yl; Ad^{dmf} = N^6-(dimethylamino)methyleneadenin-9-yl; $Gu^{ce,pac}$ = O^6-cyanoethyl-N^2-phenoxyacetylguanin-9-yl.

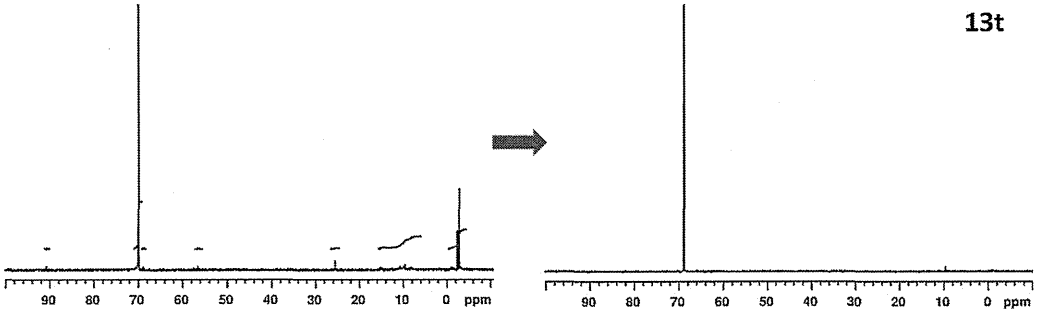

Fig. 1. ^{31}P NMR spectra of crude **13t** (left) and **13t** purified by FSPE (right).

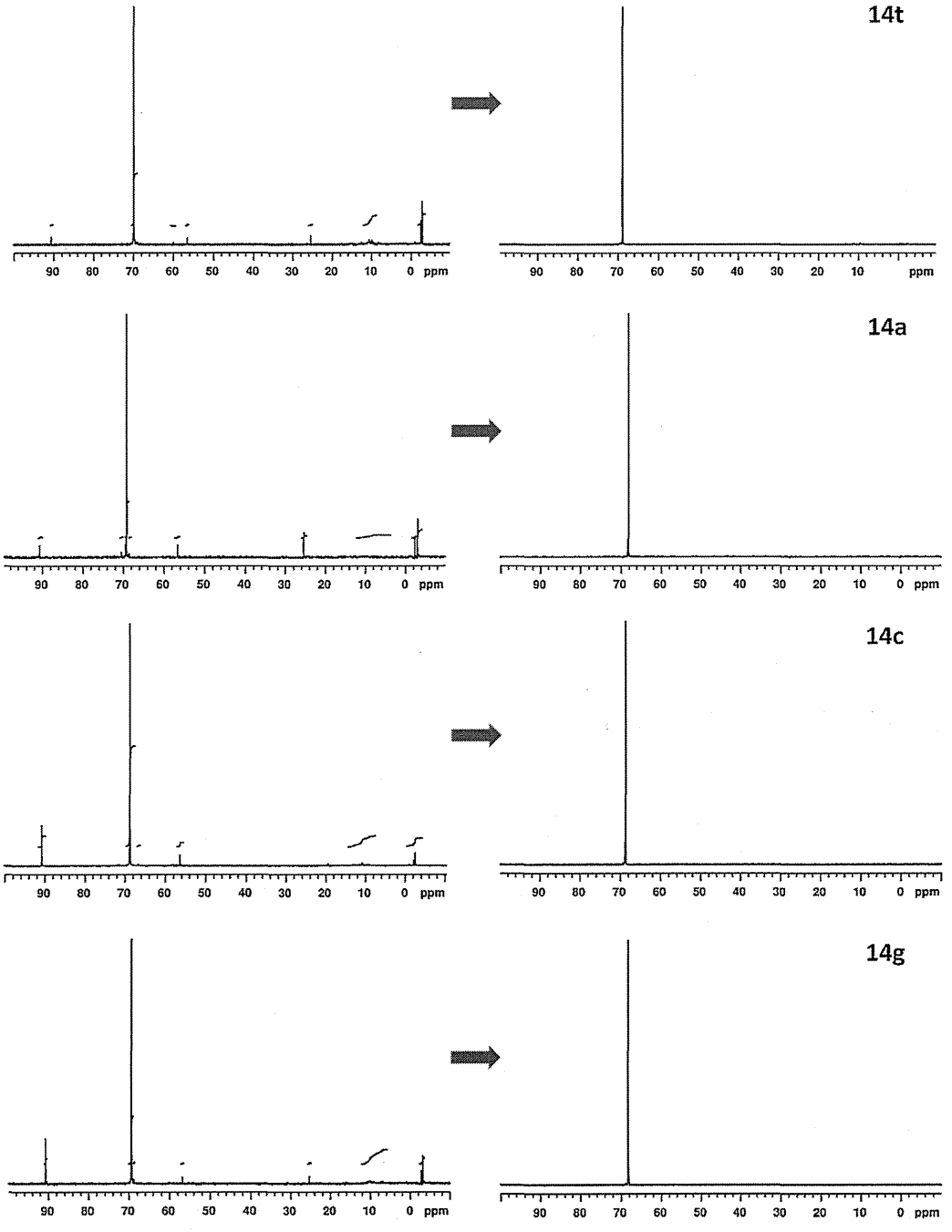

Fig. 2. ^{31}P NMR spectra of crude **14t**,**a**,**c**,**g** (left) and of those purified by FSPE (right).

[12c,d], because the fluorine contents of **5a–c** are relatively low (19–29 wt%) due to the large non-fluorous 4,4′-DMTr group and they might be useful as model compounds of the corresponding fluorous-tagged di- or oligonucleoside phosphorothioates. When **5a,b** were loaded onto a short fluorous silica gel column and washed with a non-fluorous solvent (methanol–H_2O (8:2, v/v)), they were sufficiently retained in the column. In contrast, **5c** bearing a C_4F_9 group was mostly eluted from the column, indicating that the C_4F_9 tag was not useful for this method. Therefore, the former two compounds were employed for further study on the fluorous synthesis of stereoregulated dinucleoside phosphorothioates by the oxazaphospholidine method. Compounds **5a,b** were treated with 3 vol% dichloroacetic acid (DCA) to give the fluorous-tagged thymidine derivatives having a free 5′-OH group (**6a,b**) (Scheme 2).

Next, we investigated the stereocontrolled synthesis of dinucleoside phosphorothioates using the fluorous tags (Scheme 3). First, the thymidine derivative tagged with a C_8F_{17} group (**6a**) was reacted with a thymidine 3′-*O*-oxazaphospholidine derivative (**7t**) [8d] in the presence of *N*-(cyanomethyl)pyrrolidinium triflate (CMPT, **8**) [8b] in dry MeCN to give the dinucleoside phosphite intermediate **9t**. Subsequent *N*-trifluoroacetylation with *N*-(trifluoroacetyl)imidazole, *P*-sulfurization with *N,N′*-dimethylthiuram disulfide (DTD) [17] and 5′-detritylation with DCA in the presence of Et_3SiH as a trityl cation scavenger [18] gave the fluorous-tagged dithymidine phosphorothioate triester intermediate **13t**. The whole process from **6a** to **13t** was carried out without purification of the intermediates. The intermediate **13t** was then purified by FSPE. A ^{31}P NMR analysis showed that the same FSPE procedure as attempted with **5a,b** completely removed the residues of the oxazaphospholidine monomer and any other phosphorus-containing byproducts (Fig. 1). The intermediate **13t** was not observed in the non-fluorous eluent and the recovery of **13t** was virtually quantitative.

The thymidine derivative bearing a C_6F_{13} tag **6b** was also used for the synthesis of dinucleoside phosphorothioates (Scheme 3). The same procedure as for **6a** was employed; the only difference between **6a** and **6b** was the solubility in MeCN; **6a** can be dissolved in MeCN only at a low concentration (0.056 M), whereas **6b** can be dissolved at a higher concentration (e.g., 0.1 M). The one-pot procedure gave the four kinds of dinucleoside phosphorothioate triester intermediates **14t,a,c,g**,

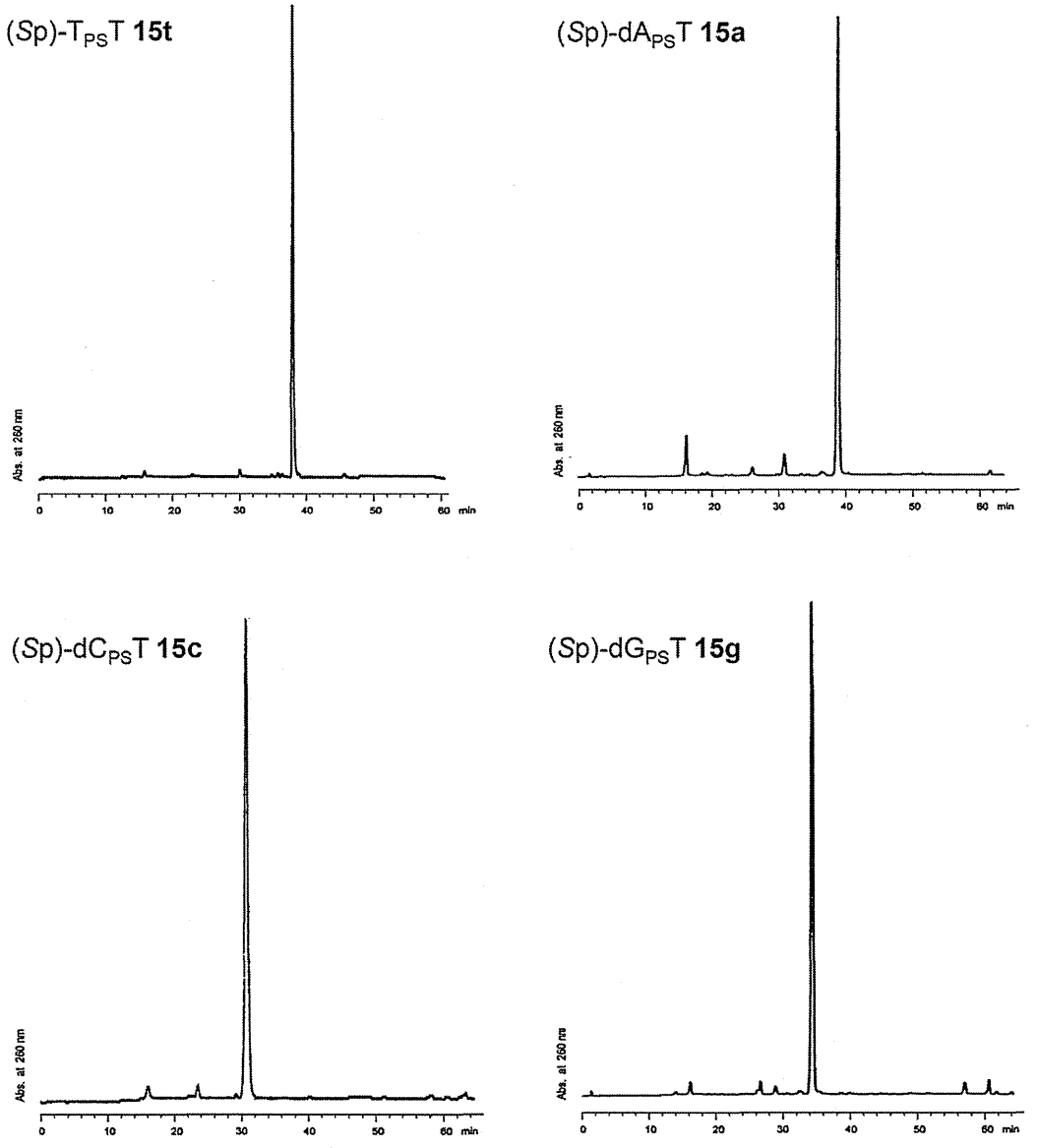

Fig. 3. RP-HPLC profiles of crude dinucleoside phosphorothioates **15t,a,c,g**.

which were then purified by FSPE. As in the case of **6a**, all of these intermediates were well-purified by FSPE (Fig. 2). The purified **14t,a,c,g** obtained from **6b** were then treated with concentrated ammonia at an elevated temperature to remove the base protecting groups, the chiral auxiliary at the phosphorothioate linkage and the fluorous tag. The resultant products were washed with $CHCl_3$ to remove any hydrophobic materials and analyzed by RP-HPLC with authentic samples synthesized by the method we previously reported [8d] (Fig. 3). The analysis showed that the desired (*Sp*)-dinucleoside phosphorothioates were obtained in good to excellent yields. The diastereopurity of the dinucleoside phosphorothioates was as high as that obtained by the previously reported synthesis on solid-support (>99:1).

3. Conclusion

In conclusion, diastereopure dinucleoside phosphorothioates were synthesized in a stereocontrolled manner by using thymidine derivatives bearing a simple perfluoroalkyl tag at the 3′-end and the diastereopure nucleoside 3′-*O*-oxazaphospholidine monomers. The thymidine derivatives having a C_6F_{13} or a C_8F_{17} group attached to the 3′-OH via a succinate linker have sufficient solubility in organic solvents and affinity to fluorous silica gel so that they can be used for syntheses in homogeneous media and the intermediates of the synthesis can be purified by a simple FSPE procedure. Further studies on the applicability of this method to the synthesis of oligodeoxyribonucleoside phosphorothioates are in progress.

4. Experimental

4.1. General

All NMR spectra were recorded on a Varian Mercury 300. ^{1}H NMR spectra were obtained at 300 MHz with tetramethylsilane (TMS) (δ 0.0) as an internal standard in $CDCl_3$. ^{13}C NMR spectra were obtained at 75 MHz with $CDCl_3$ as an internal standard (δ 77.0) in $CDCl_3$ or with pyridine-d_5 as an internal standard (δ 123.5) in pyridine-d_5. ^{31}P NMR spectra were obtained at 121.5 MHz with 85% H_3PO_4 (δ 0.0) as an external standard in $CDCl_3$. ESI mass spectra were recorded on an Applied Biosystems QSTAR. Dry organic solvents were prepared by appropriate procedures. The other organic solvents were reagent grade and used as received. Silica gel column chromatography was carried out using Kanto silica gel 60N (spherical, neutral, 63–210 μm). FSPE was carried out by using FluoroFlash® Silica Gel, 40 μm (Fluorous Technologies, Inc.).

4.2. General procedure for synthesis of 5a–c

Compound **4** (0.375 g, 0.50 mmol) was dried by repeated coevaporations with dry pyridine and dissolved in dry dichloromethane (5.0 mL) under Ar. Dry pyridine (0.12 mL, 1.5 mmol), 3-(perfluoroalkyl)propanol (perfluoroalkyl = C_8F_{17}, C_6F_{13} or C_4F_9) (0.55 mmol), and MNTP (0.537 g, 1.2 mmol) were added, and the mixture was stirred for 12 h at rt. The mixture was then diluted with $CHCl_3$ (30 mL) and washed with saturated $NaHCO_3$ aqueous solutions (3 × 20 mL). The aqueous layers were combined and back-extracted with $CHCl_3$ (2 × 10 mL). The organic layers were combined, dried over Na_2SO_4, filtered and concentrated under reduced pressure. The residue was purified by silica gel column chromatography [2.7 cm id, 27 g of silica gel, dichloromethane–methanol–pyridine (100:0:0.5 then 100:1:0.5, v/v/v)] to afford **5a**, **b** or **c**.

4.3. Compound 5a (Rf = $(CH_2)_3C_8F_{17}$)

0.517 g (0.47 mmol, 94%) of **5a** was obtained as a colorless foam from 0.375 g (0.50 mmol) of **4**. ^{1}H NMR (300 MHz, $CDCl_3$) δ 9.51 (s, 1H, 3-H of thymine), 7.62 (s, 1H, 6-H of thymine), 7.41–7.24 (m, 9H, meta to OCH_3, ArH of DMTr), 6.84 (d, $^3J_{HH}$ = 8.1 Hz, 4H, ortho to OCH_3), 6.47 (t, $^3J_{HH}$ = 7.1 Hz, 1H, 1′-H), 5.49 (s, 1H, 3′-H), 4.18 (t, $^3J_{HH}$ = 6.5 Hz, 2H, OCH_2), 4.15 (s, 1H, 4′-H), 3.79 (s, 6H, OCH_3 of DMTr), 3.48 (s, 2H, 5′-H), 2.66 (s, 4H, CH_2 of succinate), 2.48–2.44 (m, 2H, 2′-H), 2.27–2.10 (m, 2H, CF_2CH_2), 2.01–1.94 (m, 2H, $CF_2CH_2CH_2$), 1.37 (s, 3H, 5-CH_3). ^{13}C NMR (75 MHz, $CDCl_3$) δ 172.2, 172.0, 164.2, 159.0, 151.0, 144.4, 135.6, 135.5, 135.3, 130.3, 130.3, 128.4, 128.3, 127.4, 122–104 (indistinguishable cluster of peaks due to CF_x groups), 113.5, 112.0, 87.4, 84.5, 84.2, 76.2, 64.0, 63.6, 55.4, 38.1, 29.2, 28.9, 28.0 (t, $^2J_{CF}$ = 22.5 Hz), 20.1, 11.8. ESI-HRMS: *m/z* calcd for $C_{46}H_{42}F_{17}N_2O_{10}^+$ [(M+H)$^+$] 1105.2563, found 1105.2550.

4.4. Compound 5b (Rf = $(CH_2)_3C_6F_{13}$)

0.486 g (0.48 mmol, 81%) of **5b** was obtained as a colorless foam from 0.449 g (0.60 mmol) of **4**. ^{1}H NMR (300 MHz, $CDCl_3$) δ 9.39 (s, 1H, 3-H of thymine), 7.62 (s, 1H, 6-H of thymine), 7.40–7.25 (m, 9H, meta to OCH_3, ArH of DMTr), 6.84 (d, $^3J_{HH}$ = 7.8 Hz, 4H, ortho to OCH_3), 6.47 (t, $^3J_{HH}$ = 7.1 Hz, 1H, 1′-H), 5.49 (s, 1H, 3′-H), 4.19 (t, $^3J_{HH}$ = 6.5 Hz, 2H, OCH_2), 4.15 (s, 1H, 4′-H), 3.79 (s, 6H, OCH_3 of DMTr), 3.48 (s, 2H, 5′-H), 2.67 (s, 4H, CH_2 of succinate), 2.49–2.44 (m, 2H, 2′-H), 2.27–2.10 (m, 2H, CF_2CH_2), 2.02–1.91 (m, 2H, $CF_2CH_2CH_2$), 1.36 (s, 3H, 5-CH_3). ^{13}C NMR (75 MHz, $CDCl_3$) δ 172.3, 172.1, 164.4, 159.0, 151.1, 144.4, 135.6, 135.5, 135.3, 130.3, 128.4, 128.3, 127.4, 122–106 (indistinguishable cluster of peaks due to CF_x groups), 113.5, 112.0, 87.4, 84.5, 84.2, 76.2, 64.0, 63.6, 55.4, 38.0, 29.2, 28.9, 28.0 (t, $^2J_{CF}$ = 22.4 Hz), 20.1, 11.8. ESI-HRMS: *m/z* calcd for $C_{44}H_{42}F_{13}N_2O_{10}^+$ [(M+Na)$^+$] 1027.2446, found 1027.2436.

4.5. Compound 5c (Rf = $(CH_2)_3C_4F_9$)

0.202 g (0.22 mmol, 75%) of **5c** was obtained as a colorless foam from 0.224 g (0.30 mmol) of **4**. ^{1}H NMR (300 MHz, $CDCl_3$) δ 9.56 (s, 1H, 3-H of thymine), 7.62 (s, 1H, 6-H of thymine), 7.40–7.24 (m, 9H, meta to OCH_3, ArH of DMTr), 6.84 (d, $^3J_{HH}$ = 7.8 Hz, 4H, ortho to OCH_3), 6.47 (t, $^3J_{HH}$ = 7.2 Hz, 1H, 1′-H), 5.49 (s, 1H, 3′-H), 4.20–4.14 (m, 3H, 4′-H, OCH_2), 3.79 (s, 6H, OCH_3 of DMTr), 3.47 (s, 2H, 5′-H), 2.66 (s, 4H, CH_2 of succinate), 2.48–2.44 (m, 2H, 2′-H), 2.27–2.09 (m, 2H, CF_2CH_2), 2.01–1.92 (m, 2H, $CF_2CH_2CH_2$), 1.36 (s, 3H, 5-CH_3). ^{13}C NMR (75 MHz, $CDCl_3$) δ 172.0, 171.7, 163.7, 158.7, 150.5, 144.1, 135.3, 135.2, 135.0, 130.1, 128.1, 128.0, 127.2, 122–106 (indistinguishable cluster of peaks due to CF_x groups), 113.2, 111.7, 87.2, 84.2, 83.9, 76.0, 63.7, 63.3, 55.2, 37.8, 29.0, 28.7, 27.6 (t, $^2J_{CF}$ = 22.4 Hz), 19.8, 11.5. ESI-HRMS: *m/z* calcd for $C_{42}H_{42}F_9N_2O_{10}^+$ [(M+H)$^+$] 905.2690, found 905.2671.

4.6. Compound 6a (Rf = $(CH_2)_3C_8F_{17}$)

6 vol% DCA solution in dichloromethane (25 mL) was added to a stirred solution of compound **5a** (0.517 g, 0.47 mmol) in dichloromethane (25 mL) at rt. The mixture was then stirred for 20 min at rt and washed with saturated $NaHCO_3$ aqueous solutions (3 × 30 mL). The aqueous layers were combined and back-extracted with dichloromethane (2 × 20 mL). The organic layers were combined, dried over Na_2SO_4, filtered and concentrated under reduced pressure. The residue was purified by silica gel column chromatography [2.2 cm id, 15 g of silica gel, dichloromethane–methanol (100:0 then 100:3, v/v)] to afford **6a** (0.358 g, 0.45 mmol, 95%) as a colorless solid. ^{1}H NMR (300 MHz, $CDCl_3$) δ 8.13 (s, 1H, 3-H of thymine), 7.49 (s, 1H, 6-H of thymine), 6.23

(t, $^3J_{HH}$ = 7.1 Hz, 1H, 1′-H), 5.39 (s, 1H, 3′-H), 4.20 (t, $^3J_{HH}$ = 6.0 Hz, 2H, OCH_2), 4.11 (s, 1H, 4′-H), 3.93 (s, 2H, 5′-H), 2.67 (s, 4H, CH_2 of succinate), 2.45–2.40 (m, 2H, 2′-H), 2.22–2.11 (m, 2H, CF_2CH_2), 2.00–1.97 (m, 2H, $CF_2CH_2CH_2$), 1.93 (s, 3H, 5-CH_3). ^{13}C NMR (75 MHz, pyridine-d_5) δ 172.5, 172.3, 164.8, 151.9, 136.1, 120–106 (indistinguishable cluster of peaks due to CF_x groups), 110.9, 86.0, 84.9, 76.6, 63.4, 62.4, 37.8, 29.5, 29.2, 27.7 (t, $^2J_{CF}$ = 21.9 Hz), 20.2, 12.7. ESI-HRMS: *m/z* calcd for $C_{25}H_{24}F_{17}N_2O_8^+$ [(M+H)$^+$] 803.1256, found 803.1209.

4.7. Compound **6b** (*Rf* = $(CH_2)_3C_6F_{13}$)

6 vol% DCA solution in dichloromethane (25 mL) was added to a stirred solution of compound **5b** (0.486 g, 0.48 mmol) in dichloromethane (25 mL) at rt. The mixture was then stirred for 20 min at rt and washed with saturated $NaHCO_3$ aqueous solutions (3 × 50 mL). The aqueous layers were combined and back-extracted with dichloromethane (30 mL). The organic layers were combined, dried over Na_2SO_4, filtered and concentrated under reduced pressure. The residue was purified by silica gel column chromatography [2.2 cm id, 17 g of silica gel, dichloromethane–methanol (100:0 then 100:2.5, v/v)] to afford **6b** (0.325 g, 0.46 mmol, 95%) as a colorless solid. ^1H NMR (300 MHz, $CDCl_3$) δ 9.82 (s, 1H, 3-H of thymine), 7.61 (s, 1H, 6-H of thymine), 6.28 (t, $^3J_{HH}$ = 7.1 Hz, 1H, 1′-H), 5.40 (s, 1H, 3′-H), 4.20 (t, $^3J_{HH}$ = 6.0 Hz, 2H, OCH_2), 4.11 (s, 1H, 4′-H), 3.91 (s, 2H, 5′-H), 3.36 (s, 1H, OH), 2.68 (s, 4H, CH_2 of succinate), 2.48–2.40 (m, 2H, 2′-H), 2.26–2.11 (m, 2H, CF_2CH_2), 2.03–1.93 (m, 2H, $CF_2CH_2CH_2$), 1.91 (s, 3H, 5-CH_3). ^{13}C NMR (75 MHz, $CDCl_3$) δ 172.4, 172.3, 164.5, 151.0, 136.8, 124–104 (indistinguishable cluster of peaks due to CF_x groups), 111.5, 86.1, 85.3, 75.5, 63.6, 62.6, 37.4, 29.1, 28.9, 27.9 (t, $^2J_{CF}$ = 22.5 Hz), 20.1, 12.7. ESI-HRMS: *m/z* calcd for $C_{23}H_{24}F_{13}N_2O_8^+$ [(M+H)$^+$] 703.1320, found 703.1308.

4.8. Stereocontrolled synthesis of dithymidine phosphorothioate triester intermediate **13t**

The thymidine 3′-*O*-oxazaphospholidine derivative **7t** (75.5 mg, 0.10 mmol) was dried by coevaporation with dry MeCN (3 mL) under Ar and dissolved in a 0.3 M solution of CMPT **8** (0.5 mL), which was dried over MS3A overnight. The resultant solution was added to the compound **6a** (40.1 mg, 50 μmol), which was dried by coevaporation with dry MeCN prior to use, and the resultant mixture was stirred for 20 min at rt under Ar. *N*-(Trifluoroacetyl)imidazole (17.0 μL, 0.15 mmol) and *i*-Pr_2NEt (44.0 μL, 0.25 mmol) were added and the mixture was stirred for 30 min at rt. Then DTD (31.9 mg, 0.15 mmol) was added and the mixture was stirred for 50 min at rt. The mixture was then concentrated under reduced pressure, and the residue was dissolved in dichloromethane (5.0 mL). A 6 vol% DCA solution in dichloromethane (5.0 mL) and Et_3SiH (1.2 mL, 7.5 mmol) were added and the mixture was stirred for 20 min at rt. The mixture was washed with saturated $NaHCO_3$ aqueous solutions (3 × 10 mL). The aqueous layers were combined and back-extracted with dichloromethane (2 × 10 mL). The organic layers were combined, dried over Na_2SO_4, filtered and concentrated under reduced pressure. The residue was purified by FSPE [1.6 cm column id, 4.8 g of fluorous silica gel, methanol–H_2O 16 mL (80:20, v/v) then THF 25 mL] to give **13t** (73.3 mg, colorless foam), which was analyzed by ^{31}P NMR (121 MHz, $CDCl_3$) δ 68.9.

4.9. General procedure for stereocontrolled synthesis of (Sp)-$dN_{PS}T$ **15t,a,c,g** from **6b**

The compound **6b** (35.1 mg, 50 μmol) was dried by repeated coevaporations with dry MeCN (3 mL) under Ar. The thymidine 3′-*O*-oxazaphospholidine derivative **7t** (75.5 mg, 0.10 mmol), which was dried in vacuo overnight, and a 0.3 M solution of CMPT **8** (0.5 mL), which was dried over MS3A overnight, were successively added, and the mixture was stirred for 20 min at rt under Ar. *N*-(Trifluoroacetyl)imidazole (17.0 μL, 0.15 mmol) and *i*-Pr_2NEt (44.0 μL, 0.25 mmol) were added and the mixture was stirred for 30 min at rt. Then DTD (31.9 mg, 0.15 mmol) was added and the mixture was stirred for 50 min at rt. The mixture was then concentrated under reduced pressure, and the residue was dissolved in dichloromethane (5.0 mL). A 6 vol% DCA solution in dichloromethane (5.0 mL) and Et_3SiH (1.2 mL, 7.5 mmol) were added and the mixture was stirred for 20 min at rt. The mixture was washed with saturated $NaHCO_3$ aqueous solutions (3 × 10 mL). The aqueous layers were combined and back-extracted with dichloromethane (2 × 10 mL). The organic layers were combined, dried over Na_2SO_4, filtered and concentrated under reduced pressure. The residue was purified by FSPE [1.6 cm column id, 4.8 g of fluorous silica gel, methanol–H_2O 16 mL (80:20, v/v) then THF 25 mL] to give **14t**, **a**, **c** or **g** as a colorless foam, which was analyzed by ^{31}P NMR (Fig. 2). The **14t**, **a**, **c** or **g** thus obtained was dissolved in ethanol (8.0 mL) and a 25% NH_3 aqueous solution (40 mL) was added. The mixture was put in a sealed flask and heated at 55 °C for 12 h while stirring. The mixture was then cooled to rt, concentrated under reduced pressure to ca. 20 mL The mixture was diluted with a 0.1 M ammonium acetate buffer (pH 7.0) (20 mL) and washed with $CHCl_3$ (4 × 20 mL). The aqueous layer was then concentrated under reduced pressure. The residue was repeatedly lyophilized from distilled H_2O to remove ammonium acetate to give crude the dinucleoside phosphorothioate (**15t**, **a**, **c** or **g**), which was analyzed by RP-HPLC [Senshu Pak PEGASIL ODS, 4 × 150 mm, linear gradient of 0–20% MeCN (60 min) in 0.1 M triethylammonium acetate buffer (pH 7.0), 50 °C, 0.5 mL/min]. Authentic samples of **15t,a,c,g** were synthesized via the solid-phase synthesis using the nucleoside 3′-*O*-oxazaphospholidines **7t,a,c,g** as monomer units [8d].

Acknowledgments

We thank Professor Kazuhiko Saigo (Kochi University of Technology) for helpful suggestions and Ms. Sakie Hirochi for her skilled technical assistance. This research was supported by grants from the Ministry of Education, Culture, Sports, Science and Technology (MEXT) Japan.

References

[1] (a) C. Wilson, A.D. Keefe, Curr. Opin. Chem. Biol. 10 (2006) 607–614;
(b) D. Bumcrot, M. Manoharan, V. Koteliansky, D.W.Y. Sah, Nat. Chem. Biol. 2 (2006) 711–719;
(c) E.R. Rayburn, R. Zhang, Drug Discov. Today 13 (2008) 513–521.
[2] (a) A. Okamoto, Y. Saito, I.J. Saito, Photochem. Photobiol. C: Photochem. Rev. 6 (2005) 108–122;
(b) U. Asseline, Curr. Org. Chem. 10 (2006) 491–518.
[3] (a) A. Condon, Nat. Rev. Genet. 7 (2006) 565–575;
(b) N.C. Seeman, Mol. Biotechnol. 37 (2007) 246–257;
(c) F.A. Aldaye, A.L. Palmer, H.F. Sleiman, Science 321 (2008) 1795–1799.
[4] Y. Xu, H. Sugiyama, Angew. Chem. Int. Ed. 45 (2006) 1354–1362.
[5] M.A. Valencia-Sanchez, J.D. Liu, G.J. Hannon, R. Parker, Genes Dev. 20 (2006) 515–524.
[6] (a) A. Fire, S. Xu, M.K. Montgomery, S.A. Kostas, S.E. Driver, C.C. Mello, Nature 391 (1998) 806–811;
(b) S.M. Elbashir, J. Harborth, W. Lendeckel, A. Yalcin, K. Weber, T. Tuschl, Nature 411 (2001) 494–498.
[7] (a) R.C. Lee, R.L. Feinbaum, V. Ambros, Cell 75 (1993) 843–854;
(b) B. Wightman, I. Ha, G. Ruvkun, Cell 75 (1993) 855–862.
[8] (a) N. Oka, T. Wada, K. Saigo, J. Am. Chem. Soc. 124 (2002) 4962–4963;
(b) N. Oka, T. Wada, K. Saigo, J. Am. Chem. Soc. 125 (2003) 8307–8317;
(c) T. Wada, Y. Maizuru, M. Shimizu, N. Oka, K. Saigo, Bioorg. Med. Chem. Lett. 16 (2006) 3111–3114;
(d) N. Oka, M. Yamamoto, T. Sato, T. Wada, J. Am. Chem. Soc. 130 (2008) 16031–16037;

(e) N. Iwamoto, N. Oka, T. Sato, T. Wada, Angew. Chem. Int. Ed. 48 (2009) 496–499;
(f) N. Oka, T. Kondo, S. Fujiwara, Y. Maizuru, T. Wada, Org. Lett. 11 (2009) 967–970;
(g) N. Oka, T. Wada, Chem. Soc. Rev. 40 (2011) 5829–5843;
(h) N. Iwamoto, N. Oka, T. Wada, Tetrahedron Lett. 53 (2012) 4361–4364;
(i) Y. Nukaga, K. Yamada, T. Ogata, N. Oka, T. Wada, J. Org. Chem. 77 (2012) 7913–7922.
[9] (a) A.A. Levin, Biochim. Biophys. Acta 1489 (1999) 69–84;
(b) F. Eckstein, Antisense Nucleic Acids Drug Dev. 10 (2000) 117–121;
(c) B. Nawrot, B. Rebowska, O. Michalak, M. Bulkowski, D. Blaziak, P. Guga, W.J. Stec, Pure Appl. Chem. 80 (2008) 1859–1871;
(d) P. Guga, M. Koziołkiewicz, Chem. Biodivers. 8 (2011) 1642–1681.
[10] P. Li, Z.A. Sergueeva, M. Dobrikov, B.R. Shaw, Chem. Rev. 107 (2007) 4746–4796.
[11] (a) R.P. Iyer, D. Yu, N.-H. Ho, W. Tan, S. Agrawal, Tetrahedron: Asymmetry 6 (1995) 1051–1054;
(b) R.P. Iyer, M.-J. Guo, D. Yu, S. Agrawal, Tetrahedron Lett. 39 (1998) 2491–2494;
(c) D. Yu, E.R. Kandimalla, A. Roskey, Q. Zhao, L. Chen, J. Chen, S. Agrawal, Bioorg. Med. Chem. 8 (2000) 275–284;
(d) A. Wilk, A. Grajkowski, L.R. Phillips, S.L. Beaucage, J. Am. Chem. Soc. 122 (2000) 2149–2156.
[12] (a) I.T. Horváth, J. Rávai, Science 266 (1994) 72–75;
(b) A. Studer, S. Hadida, R. Ferritto, S.-Y. Kim, P. Jeger, P. Wipf, D.P. Curran, Science 275 (1997) 823–826;
(c) D.P. Curran, S. Hadida, M. He, J. Org. Chem. 62 (1997) 6714–6715;
(d) D.P. Curran, Z. Luo, J. Am. Chem. Soc. 121 (1999) 9069–9072.
[13] (a) T. Miura, Trends Glycosci. Glycotechnol. 15 (2003) 351–358;
(b) W. Zhang, C. Cai, Chem. Commun. (2008) 5686–5694.
[14] (a) D.P. Curran, R. Ferritto, Y. Hua, Tetrahedron Lett. 39 (1998) 4937–4940;
(b) T. Miura, Y. Hirose, M. Ohmae, T. Inazu, Org. Lett. 3 (2001) 3947–3950;
(c) L. Manzoni, Chem. Commun. (2003) 2930–2931;
(d) P.C. de Visser, M. van Helden, D.V. Filippov, G.A. van der Marel, J.W. Drijfhout, J.H. van Boom, D. Noort, H.S. Overkleeft, Tetrahedron Lett. 44 (2003) 9013–9016;
(e) L. Manzoni, R. Castelli, Org. Lett. 8 (2006) 955–957.
[15] (a) C. Beller, W. Bannwarth, Helv. Chim. Acta 88 (2005) 171–179;
(b) S. Tripathi, K. Misra, Y.S. Sanghvi, Org. Prep. Proc. Int. 37 (2005) 257–263;
(c) W.H. Pearson, D.A. Berry, P. Stoy, K.-Y. Jung, A.D. Sercel, J. Org. Chem. 70 (2005) 7114–7122;
(d) R. Mishra, S. Mishra, K. Misra, Chem. Lett. 35 (2006) 1184–1185.
[16] N. Oka, M. Shimizu, K. Saigo, T. Wada, Tetrahedron 62 (2006) 3667–3673.
[17] Q. Song, Z. Wang, Y.S. Sanghvi, Nucleosides Nucleotides Nucleic Acids 22 (2003) 629–633.
[18] (a) Z.A. Sergueeva, D.S. Sergueev, B.R. Shaw, Nucleosides Nucleotides Nucleic Acids 20 (2001) 941–945;
(b) M. Shimizu, T. Wada, N. Oka, K. Saigo, J. Org. Chem. 69 (2004) 5261–5268.

Bioorganic & Medicinal Chemistry 21 (2013) 1717–1723

Contents lists available at SciVerse ScienceDirect

Bioorganic & Medicinal Chemistry

journal homepage: www.elsevier.com/locate/bmc

Synthesis and properties of cationic oligopeptides with different side chain lengths that bind to RNA duplexes

Yusuke Maeda, Rintaro Iwata, Takeshi Wada *

Department of Medical Genome Sciences, Graduate School of Frontier Sciences, The University of Tokyo, Bioscience Building 702, Kashiwanoha, Kashiwa, Chiba 277-8562, Japan

ARTICLE INFO

Article history:
Received 4 January 2013
Revised 22 January 2013
Accepted 23 January 2013
Available online 1 February 2013

Keywords:
RNA-binding peptide
Cationic peptide
Artificial peptide
RNAi drug
DDS

ABSTRACT

A series of artificial peptides bearing cationic functional groups with different side chain lengths were designed, and their ability to increase the thermal stability of nucleic acid duplexes was investigated. The peptides with amino groups selectively increased the stability of RNA/RNA duplexes, and a relationship between the side chain length and the melting temperature (T_m) of the peptide–RNA complexes was observed. On the other hand, while peptides with guanidino groups exhibited a similar tendency with respect to the peptide structure and thermal stability of RNA/RNA duplexes, those with longer side chain lengths, such as L-2-amino-4-guanidinobutyric acid (Agb) or L-arginine (Arg) oligomers, stabilized both RNA/RNA and DNA/DNA duplexes, and those with shorter side chain lengths exhibited a higher ability to selectively stabilize RNA/RNA duplexes. In addition, peptides were designed with different levels of flexibility by introducing glycine (Gly) residues into the L-2-amino-3-guanidinopropionic acid (Agp) oligomers. It was found that insertion of Gly did not affect the thermal stability of the peptide–RNA complexes, but an alternate arrangement of Gly and Agp apparently decreased the thermal stability. Therefore, in the Agp oligomer, consecutive Agp sequences are essential for increasing the stability of RNA/RNA duplexes.

1. Introduction

In recent years, increased attention has been paid to the development of nucleic acid drugs. For example, antisense oligonucleotides and RNA interference drugs (RNAi drugs) are well known molecular tools for the regulation of gene expression, in which their mechanisms of action are based on sequence specific interactions.[1] The RNAi drugs act on the target mRNA in a sequence selective manner. Thus, RNAi drugs are attractive because of their high selectivity for the target and their shorter drug development time. Therefore, siRNAs have been widely studied for therapeutic applications; however, such RNA molecules are not sufficiently effective because of their low-membrane permeability and instability in cells. To stabilize oligonucleotides against metabolic degradation, a number of chemical modifications have been proposed,[2] and RNAi drugs generally consist of double stranded RNAs (dsRNAs) with chemical modifications. A proper modification of an RNA molecule increases its stability in cells and improves its pharmacokinetic properties.[3] Another strategy for stabilizing siRNA is the use of molecules that can non-covalently bind to RNA to protect it from attack by nucleases. For example, a fusion protein of the peptide transduction domain-dsRNA binding domain was shown to effectively transport RNAi drugs into primary cells.[4] In this case, the increased thermal stability of the dsRNAs also increased their stability in cells.[5] We are thus attempting to develop RNA/RNA duplex-binding molecules that are useful as drug delivery systems (DDSs) for siRNAs.

A wide variety of RNA-binding molecules have been reported, such as aminoglycosides[6] and RNA-binding proteins.[7] In paticular, chemically modified peptides bearing different methylene lengths in the arginine or lysine residues possess diverse affinities to RNAs.[8] In our previous study, α-(1 → 4)-linked-2,6-diamino-2,6-dideoxy-D-glucopyranose oligomers were synthesized, and their highly RNA-selective binding ability was demonstrated.[9] These results suggested that the geometry of the cationic groups, particularly the distance between the cationic groups, affects the affinity and selectivity of the oligomers for nucleic acid duplexes. Therefore, in this study, we designed a series of cationic oligopeptides to reveal the relationship between the geometry of the cationic groups and the affinity of the peptides for nucleic acids. In contrast to oligosaccharide derivatives, peptides can easily be synthesized, which is advantageous for obtaining a systematic series of molecules. They can also be readily connected with other functional groups such as transporter molecules.[10] Therefore, RNA duplex-binding peptides are useful tools for the development of drug delivery systems (DDSs) for RNAi drugs. The L-arginine (Arg) oligomers designed from the HIV Tat peptide are well known for their high-membrane permeability[11] and the Arg 15mer has been used as an RNAi transporter by forming a complex with RNA.[12]

* Corresponding author. Tel.: +81 4 7136 3611.
E-mail address: wada@k.u-tokyo.ac.jp (T. Wada).

0968-0896/$ - see front matter © 2013 Elsevier Ltd. All rights reserved.
http://dx.doi.org/10.1016/j.bmc.2013.01.053

However, the activity varies with the side chain length,[13] and thus a more detailed study of the relationship between the structure and activity is important for the development of effective carriers for RNAi drugs. Thus, to investigate the structural effects on binding ability, we designed and synthesized a number of cationic oligopeptides bearing different side chain lengths to control the distance between the cationic functional groups and peptides with different flexibility by incorporating glycine (Gly).

2. Results and discussion

2.1. Design of the peptides

A series of cationic oligopeptides was designed (Fig. 1). All peptides contained a unit of *N*-acetyl-L-tyrosine with two glycine residues at the N-terminus for UV detection and quantification. In this study, the 12mer of nucleic acid duplexes was used as a model to estimate the interaction with peptides bearing four or eight cationic groups because four pairs of phosphate groups are aligned on the inward portion of the major groove of the 12mer of A-type nucleic acid duplexes. First, to compare the effects of the distance between cationic groups, peptides with different side chain lengths were designed. Peptides were synthesized with amino groups (L-2,3-diaminopropionic acid (Dap), L-2,4-diaminobutyric acid (Dab), L-ornithine (Orn), and L-lysine (Lys)) and guanidino groups (L-2-amino-3-guanidinopropionic acid (Agp), L-2-amino-4-guanidinobutyric acid (Agb), and L-arginine (Arg)). In some molecules, several glycine units were also inserted into an Agp octamer to increase the flexibility of the peptides. Peptides with alternate arrangements were also designed to change the position and combination of the functional groups. These peptides were based on the Agp oligomer and other amino acids such as glycine (Gly), L-serine (Ser), and L-asparagine (Asn). Glycine was chosen because of its high flexibility. Ser and Asn were chosen because they are well known in RNA-binding proteins to form hydrogen bonds with the phosphate groups of RNA.[14]

On the basis of molecular mechanics calculations with a GB/SA water solvation model,[15] a cationic oligopeptide 8mer consisting of Dab can bind to the major groove of an A-type RNA/RNA duplex 12mer, in which all the protonated amino groups of the peptide form the hydrogen bonds to the phosphate anions of the duplex (Fig. 2). Therefore, the electrostatic interaction and hydrogen bonding would be important for the binding of cationic oligopeptides to RNA/RNA duplexes.

2.2. Melting temperature (T_m) analysis

The T_m values of the RNA duplexes were measured both in the absence and presence of an equal amount of peptides. All measurements were performed under-physiological conditions with 10 mM phosphate buffer containing 100 mM NaCl at pH 7.0. Figure 2 shows the melting temperature enhancements and Table 1 lists the T_m values for the self complementary RNA 12mer r(CGCGAAUUCGCG)$_2$ in the absence and presence of an equal amount of peptides with amino groups. In this study, the peptides were added into the solution of nucleic acid duplexes after annealing to avoid the aggregation of the peptides at high temperature. The T_m values were affected by the side chain length, with Dab_8 (**2**) showing the highest T_m value. Comparing the Dab_8 (**2**), Orn_8 (**3**), and Lys_8 (**4**), the T_m value increased as the side chain length

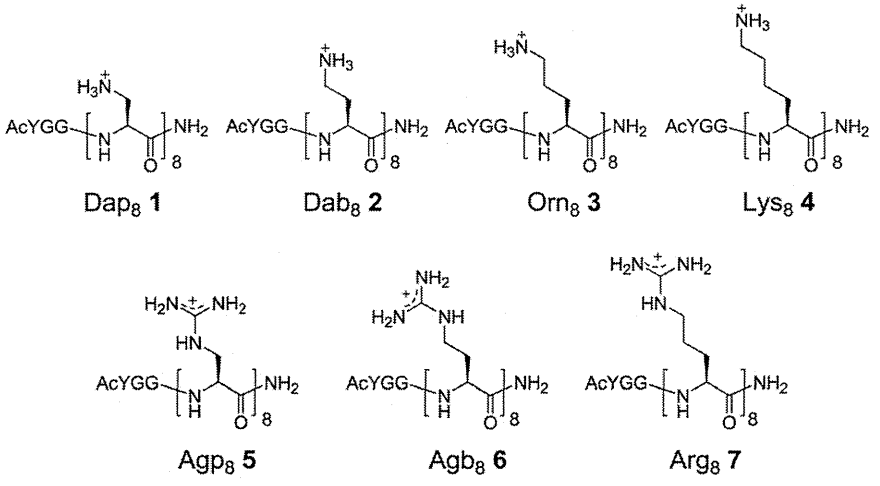

Peptides with amino groups			Peptides with flexible main chains			
Dap_8	:	Ac-YGG-Dap_8-NH_2 **1**	Agp_8G1	:	Ac-YGG-Agp_4-G-Agp_4-NH_2	**8**
Dab_8	:	Ac-YGG-Dab_8-NH_2 **2**	Agp_8G2	:	Ac-YGG-Agp_3-G-Agp_2-G-Agp_3-NH_2	**9**
Orn_8	:	Ac-YGG-Orn_8-NH_2 **3**	Agp_8G3	:	Ac-YGG-Agp_2-G-Agp_2-G-Agp_2-G-Agp_2-NH_2	**10**
Lys_8	:	Ac-YGG-Lys_8-NH_2 **4**	Agp_8A2	:	Ac-YGG-Agp_3-A-Agp_2-A-Agp_3-NH_2	**11**
Peptides with guanidino groups			Agp_8P2	:	Ac-YGG-Agp_3-P-Agp_2-P-Agp_3-NH_2	**12**
Agp_8	:	Ac-YGG-Agp_8-NH_2 **5**	**Peptides with alternate arrangement**			
Agb_8	:	Ac-YGG-Agb_8-NH_2 **6**	AgpG	:	Ac-YGG-$(Agp\text{-}G)_4$-NH_2	**13**
Arg_8	:	Ac-YGG-Arg_8-NH_2 **7**	AgpS	:	Ac-YGG-$(Agp\text{-}S)_4$-NH_2	**14**
			AgpN	:	Ac-YGG-$(Agp\text{-}N)_4$-NH_2	**15**

Figure 1. Structures and sequences of cationic peptides.

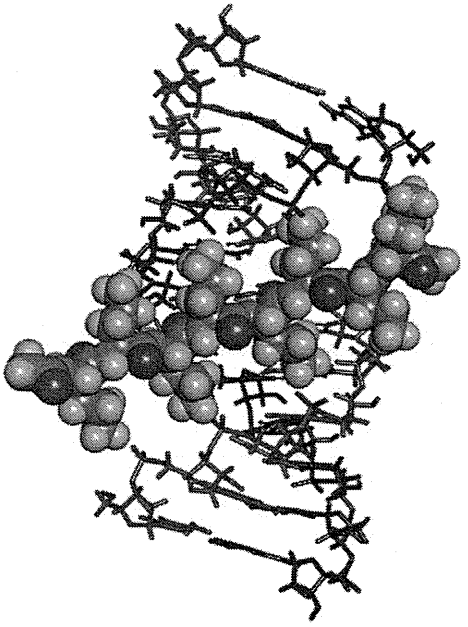

Figure 2. Molecular model of L-2,4-diaminobutylic acid (Dab) 8mer binding to A-type RNA–RNA duplex (12mer).

Table 1
Thermal melting points (T_m in °C) for oligonucleotide duplex (in the absence and presence of peptides with amino groups[a])[b]

Peptide	RNA/RNA	ΔT_m	DNA/DNA	ΔT_m
None	60.7		48.2	
Dap_8	60.2	−0.5	50.8	2.6
Dab_8	74.7	14.0	49.5	1.3
Orn_8	74.2	13.5	51.3	3.1
Lys_8	68.1	7.4	49.7	1.5

[a] Peptide concentration 4 μM.
[b] Buffer (10 mM phosphate buffere for pH 7.0), NaCl (100 mM), together with each oligonucleotide strand (4 μM). T_m values are reported at the means of duplicate measurements.

decreased. These results suggest that the distance between the amino groups in Dab_8 (**2**) fits to the distance of the opposing phosphate groups in the RNA duplexes. This tendency has been previously reported for cationic oligopeptides with D-amino acids.[6] On the other hand, Dap_8 (**1**) did not stabilize the RNA/RNA duplexes. This differing behavior may result because the distance of the amino groups in Dap_8 is too short to interact with the phosphate groups in the RNA/RNA duplexes. In fact, none of the peptides with amino groups increased the thermal stability of the DNA/DNA duplex d(CGCGAATTCGCG)$_2$ (Fig. 3). The distance between the phosphate groups in the major groove of a DNA/DNA duplex is twice that in an RNA/RNA duplex. Therefore, none of the peptides were able to interact with the DNA/DNA duplexes. In the minor groove of a DNA/DNA duplex, the interstrand phosphate groups are much closer than those in the major groove. However, the phosphate groups facing outward of the minor groove are unfavorable to form hydrogen bonds with the protonated amino groups of cationic peptides.

The peptides with guanidino groups (**5**, **6**, **7**) exhibited the same tendency as the peptides with the amino groups (Fig. 4, Table 2) for the RNA/RNA duplexes. Peptides with shorter side chain lengths had higher T_m values. This result indicates that the position of guanidino groups in Agp_8 (**5**) also fits well with the RNA duplex structure. While the distance between the functional groups is similar in the peptides with amino and guanidino groups, the peptides with

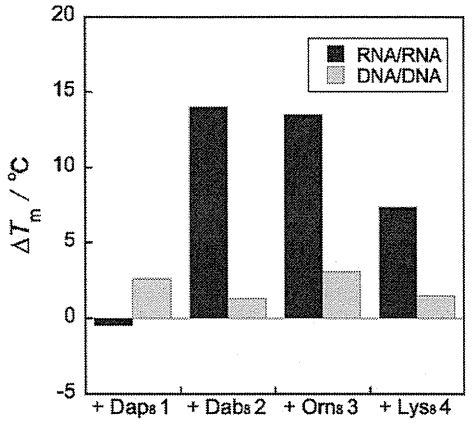

Figure 3. Melting temperature enhancements for the RNA/RNA and DNA/DNA duplexes at pH 7.0 in the presence of peptides **1–4**. Differences in the thermal melting points (ΔT_m) are given for the nucleic acid duplexes in the presence of equimolar amounts of peptide relative to the duplex alone. The dark gray columns represent ΔT_m for RNA/RNA duplex, and light gray columns represent ΔT_m values for DNA/DNA duplex.

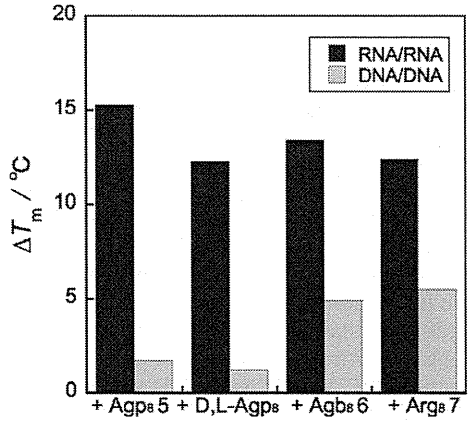

Figure 4. Melting temperature enhancements for the RNA/RNA and DNA/DNA duplexes at pH 7.0 in the presence of peptides **5–7**. Differences in the thermal melting points (ΔT_m) are given for the nucleic acid duplexes in the presence of an equal amount of peptide relative to the duplex alone. The dark gray columns represent ΔT_m for RNA/RNA duplex, and light gray columns represent ΔT_m values for DNA/DNA duplex.

Table 2
Thermal melting points (T_m in °C) for oligonucleotide duplex (in the absence and presence of peptides with guanidino groups[a])[b]

Peptide	RNA/RNA	ΔT_m	DNA/DNA	ΔT_m
None	60.7		48.2	
Agp_8	76.9	16.2	49.9	1.7
D-Agp_8	75.8	15.1	48.9	0.7
D,L-Agp_8	73.0	12.3	49.4	1.2
Agb_8	74.1	13.4	53.1	4.9
Arg_8	73.1	12.4	53.7	5.5

[a] Peptide concentration 4 μM.
[b] Buffer (10 mM phosphate buffere for pH 7.0), NaCl (100 mM), together with each oligonucleotide strand (4 μM). T_m values are reported at the means of duplicate measurements.

the guanidino groups exhibited higher T_m values. These different T_m values can be attributed to the different features of the functional groups. The guanidino group is known to have a stronger interaction with phosphate groups than amino groups, and thus the peptides with guanidino groups showed a stronger interaction

with the nucleic acid duplexes. However, in the case of the DNA/DNA duplex, the tendency changed because of the differences in the guanidino and amino functional groups. For the peptides with guanidine groups, those with longer side chain lengths had higher T_m values. This result may also be due to the fact that the guanidino groups strongly interact with the phosphate groups.

The different side chain lengths of the peptides resulted in different thermal stabilities of the nucleic acid duplexes. The duplex stability may also be affected by the flexibility of the peptides. Thus, to investigate the effect of incorporation of flexible residues into the peptide backbone, glycine was inserted into Agp_8 (**5**) to increase the flexibility of the main chain (**8**, **9**, **10**). Interestingly, it was found that an increase in the flexibility of the main chain did not affect the thermal stability of the peptide–RNA complexes (Fig. 5, Table 3). These results suggest that the stabilization of the RNA duplex with Agp_8 (**5**) is mainly attributed to enthalpic factors. In addition, insertion of L-alanine (Ala) or L-proline (Pro) into Agp_8 (**5**) also did not affect the thermal stability of the RNA duplexes (**11**, **12**). If the peptides invade the major groove, the redundant amino acid residues will give rise to steric hindrance and decrease the thermal stability. Therefore, these results suggest that the peptides interact with the surface of the nucleic acids.

Peptides with alternate arrangements also did not stabilize the RNA duplexes (Fig. 6, Table 4). Peptides consisting of Agp and Gly in an alternate arrangement, AgpG (**13**) did not have any effects on the RNA/RNA duplex. On the other hand, Agp_4 showed an appreciable stabilization effect for the RNA/RNA duplex. Therefore, a consecutive Agp sequence is effective for RNA/RNA duplex stabilization. Furthermore, Agp_8G3 (**10**), in which four Agp_2 units are connected, has the same affinity as Agp_8; thus, the Agp_2 structural unit is effective for the interaction with RNA/RNA duplexes. In Agp oligomers with a consecutive sequence, the guanidino groups are located on both sides of the peptide backbone, and this alignment is identical to that required for interaction between the guanidino groups and the phosphates in the major groove of RNA duplexes. However, peptides with a combination of guanidino and hydroxy or amide groups (AgpS (**14**) and AgpN (**15**), respectively) had no effects on the thermal stability of RNA duplexes. These results also suggest that a consecutive arrangement of cationic amino acids is essential for effective interaction with the phosphates of RNA duplexes.

The effect of chirality was also examined. The Agp oligomers consisting of all-L- and all-D-amino acids had similar T_m values,

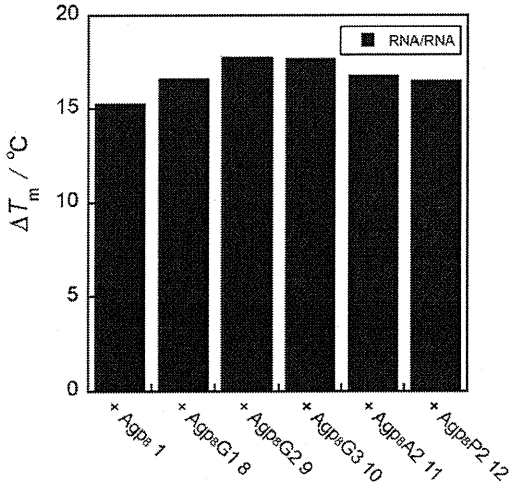

Figure 5. Melting temperature enhancements for the RNA/RNA duplexes at pH 7.0 in the presence of peptides **1**, **8–12**. Differences in the thermal melting points (ΔT_m) are given for the nucleic acid duplexes in the presence of an equal amount of peptide relative to the duplex alone.

Table 3
Thermal melting points (T_m in °C) for oligonucleotide duplex (in the absence and presence of peptides with flexible main chian[a])[b]

Peptide	RNA/RNA	ΔT_m
None	60.9	
Agp_8	77.5	16.6
Agp_8G1	77.5	16.6
Agp_8G2	78.8	17.9
Agp_8G3	78.6	17.7
Agp_8A2	77.7	16.8
Agp_8P2	77.4	16.5

[a] Peptide concentration 4 μM.
[b] Buffer (10 mM phosphate buffere for pH 7.0), NaCl (100 mM), together with each oligonucleotide strand (4 μM). T_m values are reported at the means of duplicate measurements.

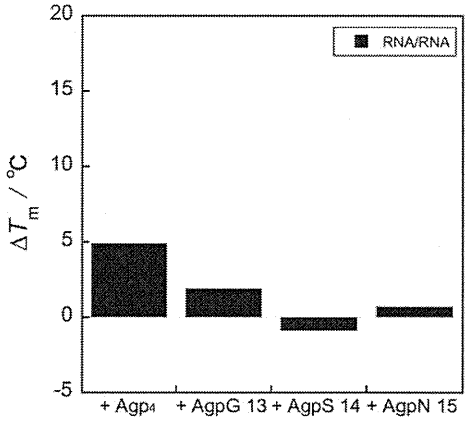

Figure 6. Melting temperature enhancements for the RNA/RNA duplexes at pH 7.0 in the presence of peptides **13–15**. Differences in the thermal melting points (ΔT_m) are given for the nucleic acid duplexes in the presence of equimolar amounts of peptide relative to the duplex alone.

Table 4
Thermal melting points (T_m in °C) for oligonucleotide duplex (in the absence and presence of peptides with alternate arrangements[a])[b]

Peptide	RNA/RNA	ΔT_m
None	60.3	
Agp_4	65.2	4.9
AgpG	62.2	1.9
AgpS	58.9	−1.4
AgpN	60.5	0.2

[a] Peptide concentration 4 μM.
[b] Buffer (10 mM phosphate buffere for pH 7.0), NaCl (100 mM), together with each oligonucleotide strand (4 μM). T_m values are reported at the means of duplicate measurements.

but the peptides having D/L-alternate arrangements slightly had lower thermal stability. A decrease in the thermal stability induced by a heterochiral backbone was also reported for chiral PNA.[16]

2.3. CD spectroscopy

The structures of the peptides and the RNA–peptide complexes in solution were analyzed using circular dichroism (CD) spectroscopy. On the basis of molecular mechanics calculations,[15] the amino groups and guanidino groups of the peptides, particularly in Dap_8 (**2**) and Agp_8 (**5**), can form intramolecular hydrogen bonds with the amido groups in the main chain. However, in the absence of nucleic acid duplexes, the spectra of all the peptides indicated the presence of random coils.[17] Therefore, the effect of the secondary structures of the peptides was negligible in these cases. The

structures of the RNA–peptide complexes were also analyzed. Because the peptides showed a variety of T_m values depending on the side chain length and the nature of the cationic functional groups, there existed not only electrostatic interactions and hydrogen bonding, but also structural factors. However, for both the RNA and DNA duplexes, no appreciable structural changes in the nucleic acids were observed following the addition of the peptides (Figs. 7 and 8). The CD spectra of the RNA and DNA duplexes in the presence and absence of peptides were typical for A-type and B-type helices, respectively.

2.4. ITC measurement

Thermodynamic analysis of the peptide–nucleic acid interactions was carried out using isothermal titration calorimetry (ITC) measurements. The duplex concentration was 2.5 times higher than that used for the UV melting analyses because the amount of heat generated during the binding between the nucleic acid duplexes and the oligocationic peptides was expected to be insufficient for calculation of the thermodynamic parameters at the lower concentration. Figures 9, S8,[17] and S9[17] show the preliminary results for the ITC titration of the peptides with the self complementary RNA/RNA duplex r(CGCGAAUUCGCG)$_2$ and DNA/DNA duplex d(CGCGAATTCGCG)$_2$. In addition to electrostatic interactions and hydrogen bonding between the peptides and nucleic acids, dehydration and dissociation of the phosphates in the buffer solution were apparently observed. Thus, the interactions were too complex for calculation of the thermodynamical parameters. However, it was observed that both of the peptides selectively interacted with the RNA/RNA duplexes. In contrast, only Agb$_8$ (**5**) interacted with both the RNA/RNA and DNA/DNA duplexes. This result may be due to the fact that, in Agb$_8$, the side chain is long and sufficiently flexible to interact with the phosphate groups of both the RNA/RNA and DNA/DNA duplexes. In comparison with the amino-substituted Dap$_8$, the guanidine-substituted Dab$_8$ (**5**) had larger endothermic interactions.

Inhibition assays were carried out to clarify the peptide-binding sites in the RNA duplexes. The peptides were titrated into a solution of the RNA duplexes in the presence of neomycin, which is known to bind to the major groove of RNA duplexes.[18] The inhibition of peptide–RNA binding by neomycin was different for the types of peptides (Fig. S10[17]). For Dab$_8$ (**2**), the exothermic interactions were selectively inhibited, while the endothermic interactions were still observed. On the other hand, for Agp$_8$ (**5**), both of the interactions were inhibited. These results suggest that the exothermic interactions are attributed to the binding of the peptides to the major groove of RNA/RNA duplexes and the endothermic interactions are related to the interactions with other sites.

3. Materials and methods

3.1. Peptide synthesis

Peptides were synthesized via a conventional solid-phase method by using the 9-fluorenylmethyloxycarbonyl (Fmoc) strategy.[19] The peptide chains were assembled on a Fmoc-NH-SAL-PEG resin by using Fmoc amino acid derivatives (5 equiv), *N,N*-diisopropylethylamine (DIPEA, 10 equiv), and 2-(1*H*-9-azabenzotriazole-1-yl)-1,1,3,3-tetramethyluronium hexafluorophosphate (HATU, 5 equiv) in dimethylformamide (DMF) for the coupling, and 25% piperidine/DMF for the removal of the Fmoc group. After coupling of the last amino acids, amino groups at the N-termini were protected with an acetyl (Ac) group using acetic anhydride (10 equiv). To cleave the peptide from the resin and remove the side chain protecting groups, the peptide resin was treated with trifluoroacetic acid (TFA)-triisopropylsilane-water, (95:2.5:2.5, v/v/v). Peptides in sat $NaHCO_{3aq}$ (200 μl) were added in one portion to a solution of the 1,3-di-Boc-2-(trifluoromethylsulfonyl)guanidine[20] (10 equiv per amino groups) in dioxane (200 μl), and stirred overnight at rt, then concentrated in vacuo. To remove the protecting groups from the guanidino groups, the peptides were treated with TFA–triisopropylsilane–water (95:2.5:2.5, v/v/v). All peptides were purified with reverse-phase HPLC (0.05% TFA in water–acetonitrile). The peptides were successfully identified by matrix-assisted laser desorption ionization time-of-flight mass spectrometry (MALDI-TOF-MS). Compound **1**, TOF-MS *m/z* calcd for $[M+Na]^+$ 1048.07; Found 1047.60. Compound **2**, TOF-MS *m/z* calcd for $[M+H]^+$ 1138.31; Found 1137.22. Compound **3**, TOF-MS *m/z* calcd for $[M+Na]^+$ 1272.50; Found 1271.56. Compound **4**, TOF-MS *m/z* calcd for $[M+H]^+$ 1362.73; Found 1361.51. Compound **5**, TOF-MS *m/z* calcd for $[M+H]^+$ 1362.41; Found 1361.51. Compound **6**, TOF-MS *m/z* calcd for $[M+H]^+$ 1474.63; Found 1473.77. Compound **7**, TOF-MS *m/z* calcd for $[M+H]^+$ 1586.84; Found 1585.72. Compound **8**, TOF-MS *m/z* calcd for $[M+H]^+$ 1419.46; Found 1418.53. Compound **9**, TOF-MS *m/z* calcd for $[M+Na]^+$ 1476.52; Found 1476.00. Compound **10**, TOF-MS *m/z* calcd for $[M+H]^+$ 1533.57; Found 1533.07. Compound **11**, TOF-MS *m/z* calcd for $[M+H]^+$ 1504.57; Found 1504.21. Compound **12**, TOF-MS *m/z* calcd for $[M+H]^+$ 1556.64; Found 1555.68. Compound **13**, TOF-MS *m/z* calcd for $[M+Na]^+$ 1100.07; Found 1099.25. Compound **14**, TOF-MS *m/z*

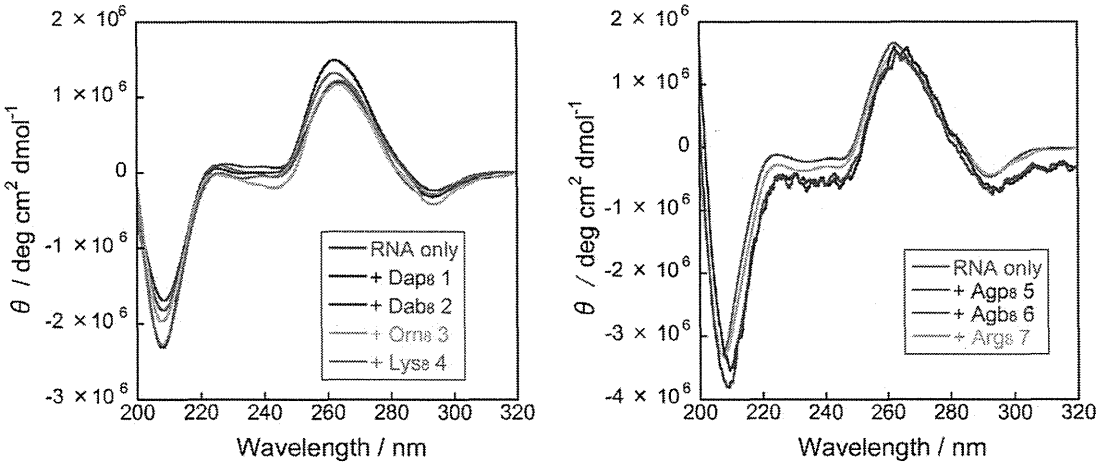

Figure 7. CD spectra of the RNA/RNA duplexes in the presence and absence of an equal amount of peptides **1–7** (at 20 °C, pH 7.0, 4 μM each of peptide and duplex).

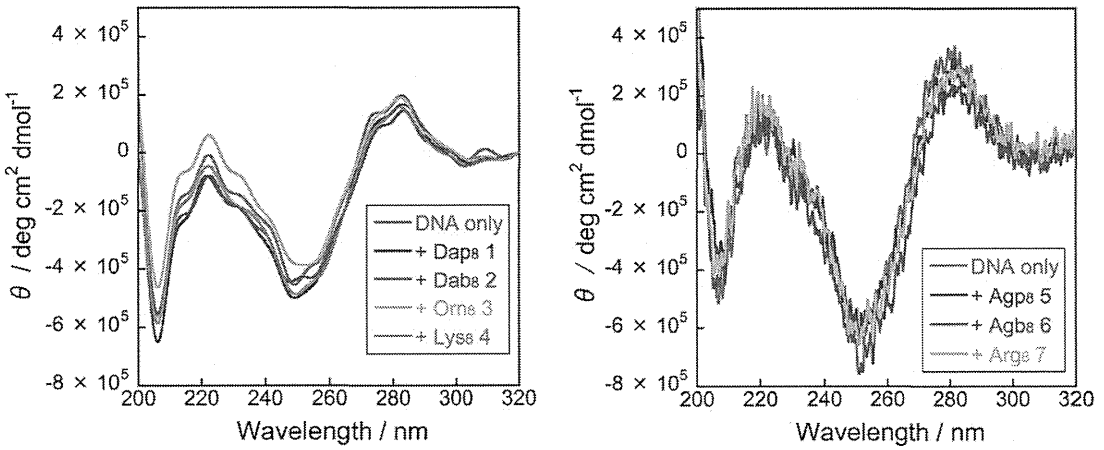

Figure 8. CD spectra of the DNA/DNA duplexes in the presence and absence of an equal amount of peptides **1–7** (at 20 °C, pH 7.0, 4 μM each of peptide and duplex).

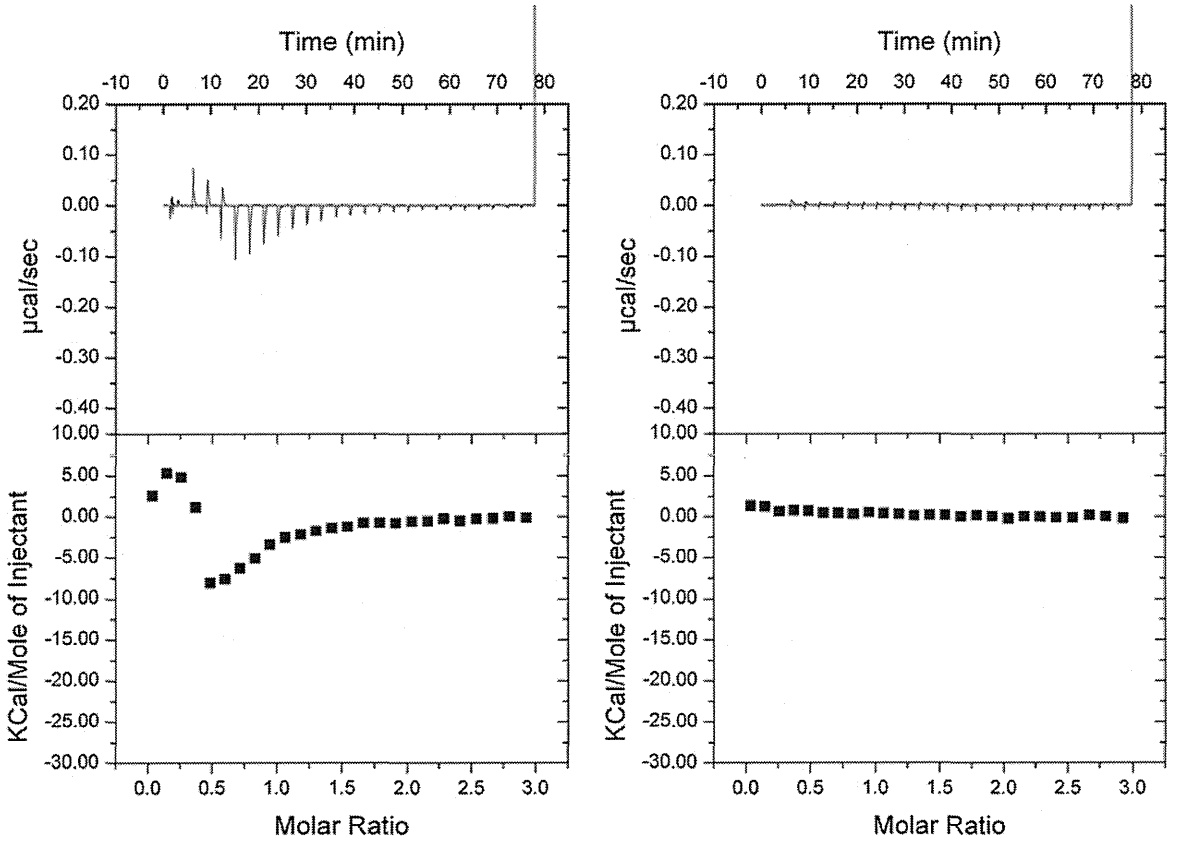

Figure 9. ITC profiles at 25 °C for titration of Dab_8 (**2**) into a solution of RNA/RNA duplex (left) and DNA/DNA duplex (right); each curve is the result of a 2.5 μl injection of 150 μM peptide. The duplex concentration was 10 μM in a 10 mM phosphate buffer with 100 mM NaCl at pH 7.0; corrected injection heat in the cases of RNA/RNA were plotted.

calcd for $[M+H]^+$ 1198.18; Found 1197.67. Compound **15**, TOF-MS *m/z* calcd for $[M+H]^+$ 1306.29; Found 1305.46.

3.2. Melting temperature (T_m) analysis

Absorbance versus temperature profile measurements were carried out in quartz cells with a 1 cm path length using an eight-sample cell changer. The variation in the UV absorbance with temperature was monitored at 260 nm. The temperature was scanned from 10 to 95 °C at a rate of 0.2 °C/min. The peptides were added after oligonucleotides were annealed. The samples were prepared as follows. The oligonucleotides were dissolved in a phosphate buffer (10 mM) containing NaCl (0.1 M) at pH 7.0. The solutions of oligonucleotides (4 μM) were first rapidly heated to 95 °C, left for 10 min, and then cooled to 10 °C at a rate of 1 °C/min. The equal amounts of peptides (final concn: 4 μM) were then added to the solution. The samples were left to equillbrate at the starting temperature for 30 min, the dissociation of the duplex was observed by heating the solution to 95 °C at a rate of 0.2 °C/min, and data points were collected at every 0.1 °C.

3.3. CD spectroscopy

All CD spectra were recorded at 20 °C. The following instrument settings were used: resolution, 0.1 nm; sensitivity, 10 mdeg; response, 4 s; speed, 10 nm/min; accumulation, 6.

3.4. Conditions for ITC experiments

The peptides and nucleic acid duplexes were dissolved in a 10 mM phosphate buffer containing 100 mM NaCl at pH 7.0. The peptide solutions (150 μM) were titrated into the nucleic acid duplex solutions (10 μM) at 25 °C. Each titration of peptide solution consisted of a preliminary 0.5 μl injection followed by 24 subsequent 1.5 μl additions, which were performed over 3 s periods at 120 s intervals. In the inhibition assays, the peptide solutions were titrated into the nucleic acid solution in the presence of 100 μM neomycin under the same conditions as described above.

4. Conclusion

We have synthesized a series of cationic oligopeptides by systematically changing the position of the cationic groups. On the basis of UV-melting analysis, CD spectrometry and ITC measurements, these cationic oligopeptides showed different tendencies for the stabilization of nucleic acid duplexes. Peptides with amino groups stabilized only RNA duplexes, while peptides with guanidino groups stabilized both RNA and DNA duplexes. In particular, Dab_8 (**2**) and Agp_8 (**5**) showed the highest T_m values among the series of peptides with the same cationic groups but different side chain length. These results suggest that the distance between the cationic groups, such as in Dab_8 (**2**) and Agp_8 (**5**), are well fitted to the distance between the phosphate groups in the major groove of RNA duplexes. Furthermore, peptides with alternate arrangements and those containing flexible amino acids did not stabilize the RNA duplexes. These results indicate that at least two consecutive sequences of Agp are necessary for effective binding of cationic oligopeptides to RNA duplexes. Therefore, given their unique properties, Dab_8 (**2**) and Agp_8 (**5**) will be useful as stabilizers of dsRNA-based nucleic acid drugs or new materials for their DDS.

Acknowledgments

We thank Professor Kohei Tsumoto (University of Tokyo) and Dr. Satoru Nagatoishi (University of Tokyo) for the ITC measurements and helpful discussions. This work was finally supported by KAKENHI and CREST, the Japan Science and Technology Agency.

Supplementary data

Supplementary data (data include CD spectra, UV melting profiles, and ITC profiles) associated with this article can be found, in the online version, at http://dx.doi.org/10.1016/j.bmc.2013.01.053.

References and notes

1. Fire, A.; Xu, S.; Montgomery, M. K.; Kostas, S. A.; Driver, S. E.; Mello, C. C. *Nature* **1998**, *391*, 806.
2. Watts, J. K.; Deleavey, G. F.; Damha, M. J. *Drug Discovery Today* **2008**, *13*, 842.
3. (a) Manoharan, M. *Biochim. Biophys. Acta* **1999**, *1489*, 117; (b) Cook, P. D. *Nucleosides Nucleotides* **1999**, *18*, 1141.
4. Eguchi, A.; Meade, B. R.; Chang, Y. C.; Fredrickson, C. T.; Williert, K.; Puri, N.; Dowdy, S. F. *Nat. Biotechnol.* **2009**, *27*, 567.
5. Prakash, T. P.; Allerson, C. R.; Vickers, T. A.; Sioufi, N.; Jarres, R.; Baker, B. F.; Swayze, E. E.; Griffey, R. H.; Bhat, B. *J. Med. Chem.* **2005**, *48*, 4247.
6. Francois, B.; Russell, R.; Murray, J. *Nucleic Acids Res.* **2005**, *33*, 5677.
7. Maris, C.; Dominguez, C.; Allain, F. H. *FEBS J.* **2005**, *272*, 2118.
8. (a) Nurtola, M.; Zaramella, S.; Yeheskiely, E.; Strömberg, R. *ChemBioChem* **2010**, *11*, 2606; (b) Wu, C. H.; Chen, Y. P.; Mou, C. Y.; Cheng, R. P. *Amino Acids* **2012**. http://dx.doi.org/10.1007/s00726-012-1357-0.
9. Iwata, R.; Sudo, M.; Nagafuji, K.; Wada, T. *J. Org. Chem.* **2011**, *76*, 5895.
10. Lemberg, M. K.; Martoglio, B. *Mol. Cell* **2002**, *10*, 735.
11. Futaki, S.; Suzuki, T.; Ohashi, W.; Yagami, T.; Tanaka, S.; Ueda, K.; Sugiura, Y. *J. Biol. Chem.* **2001**, *276*, 5836.
12. Kim, S. W.; Kim, N. Y.; Choi, Y. B.; Yang, J. M.; Shin, S. *J. Controlled Release* **2010**, *143*, 334.
13. Russell, A. L.; Williams, B. C.; Spuches, A.; Klapper, D.; Srouji, A. H.; Hicks, R. P. *Bioorg. Med. Chem.* **2012**, *20*, 1723.
14. Jones, S.; Daley, D. T.; Luscombe, N. M.; Berman, H. M.; Thornton, J. M. *Nucleic Acids Res.* **2001**, *29*, 943.
15. Mohamadi, F.; Richards, N. G. J.; Guida, W. C.; Liskamp, R.; Lipton, M.; Caufield, G.; Chang, G.; Hendrickson, T.; Still, W. C. *J. Comput. Chem.* **1990**, *143*, 334.
16. Ura, Y.; Leman, J.; Orgel, L. E.; Ghadiri, M. R. *Science* **2009**, *325*, 73.
17. See the Supplementary data.
18. Varani, L.; Spillantini, M. G.; Goedert, M.; Varani, G. *Nucleic Acids Res.* **2000**, *28*, 710.
19. *Fmoc Solid Phase Peptide Synthesis*; Chan, W. C., White, P. D., Eds.; Oxford University Press: New York, 2000. pp 42–76.
20. Xiao, S.; Fu, N.; Peckham, K.; Smith, B. D. *Org. Lett.* **2010**, *12*, 140.

Organic & Biomolecular Chemistry

PAPER

View Article Online
View Journal | View Issue

Photoinduced changes in hydrogen bonding patterns of 8-thiopurine nucleobase analogues in a DNA strand†

Cite this: *Org. Biomol. Chem.*, 2014, **12**, 2468

Kunihiko Morihiro,[a,b] Tetsuya Kodama,[c] Shohei Mori[a] and Satoshi Obika*[a,b]

Received 5th December 2013,
Accepted 13th February 2014

DOI: 10.1039/c3ob42427h

www.rsc.org/obc

Hydrogen bonds (H-bonds) formed between nucleobases play an important role in the construction of various nucleic acid structures. The H-donor and H-acceptor pattern of a nucleobase is responsible for selective and correct base pair formation. Herein, we describe an 8-thioadenine nucleobase analogue and an 8-thiohypoxanthine nucleobase analogue with a photolabile 6-nitroveratryl (NV) group on the sulfur atom (**SA^{NV}** and **SH^{NV}**, respectively). Light-triggered removal of the NV group causes tautomerization and a change in the H-bonding pattern of **SA^{NV}** and **SH^{NV}**. This change in the H-bonding pattern has a strong effect on base recognition by 8-thiopurine nucleobase analogues. In particular, base recognition by **SH^{NV}** is clearly shifted from guanine to adenine upon photoirradiation. These results show that a photoinduced change in the H-bonding pattern is a unique strategy for manipulating nucleic acid assembly with spatiotemporal control.

Introduction

The complementarity of natural A–T and G–C base pairs in DNA is the principal mechanism for the preservation and flow of genetic information. The hydrogen-bonding (H-bonding) patterns of the four natural nucleobases play an important role in the selective and correct formation of base pairs. These H-bonding interactions can result in the formation of higher order complexes of nucleic acids, depending on the sequence. Therefore, the control of H-bonding interactions using external stimuli is important for regulating biological processes and for the possibility of developing unique DNA-based molecular machines. Various external stimuli have been used to this end; light is an ideal trigger because the timing, location, and intensity of the irradiation can be easily controlled. Among such strategies, nucleobase caging strategies involving the installation of a photolabile group are very important. Photolabile caging groups perturb the H-bonding capabilities of the nucleobases. Photoirradiation reinstates the H-bonding capabilities and allows nucleobase interaction in the "OFF to ON" direction. Nucleobase-caged nucleosides can be widely used for the photoregulation of antisense oligodeoxynucleotides (ODNs),[1,2] siRNAs,[3,4] aptamers,[5] ribozymes[6,7] and deoxyribozymes,[8,9] diagnostic ODNs,[10] DNA architectures,[11] and DNA logic gates.[12,13]

Recently, we reported the synthesis and properties of a unique light-responsive nucleobase analogue derived from 2-mercaptobenzimidazole (**SB^{NV}**) (Fig. 1a).[14] **SB^{NV}** is modified with a photolabile 6-nitroveratryl (NV) group,[15] and the nitrogen at the 3-position serves as an H-acceptor (A). **SB^{NV}** can selectively form a base pair with guanine even before photoirradiation, unlike conventional caged nucleobases. Light-triggered removal of the NV group causes tautomerization of the nucleobase, and changes the role of the 3-nitrogen atom from H-A to H-donor (D). Following this change in the H-bonding pattern, base recognition by **SB^{NV}** can be shifted from guanine to adenine. We also demonstrated that a light-triggered strand exchange reaction targeting different mRNA fragment sequences could be achieved using ODNs containing **SB^{NV}**. These results indicate that a photoinduced change in the H-bonding pattern of a nucleobase is a good strategy for manipulating nucleic acid assemblies in a spatially and temporally controlled manner. In this paper, to further investigate the effect of this change in H-bonding pattern of nucleobases on the base recognition ability, we designed new light-responsive nucleoside analogues bearing the NV group: 8-thioadenine and 8-thiohypoxanthine (**SA^{NV}** and **SH^{NV}**, respectively;

[a]*Graduate School of Pharmaceutical Sciences, Osaka University, 1-6 Yamadaoka, Suita, Osaka 565-0871, Japan. E-mail: obika@phs.osaka-u,ac.jp; Fax: +81 6-6879-8204; Tel: +81 6-6879-8200*
[b]*National Institute of Biomedical Innovation (NIBIO), 7-6-8 Saito-Asagi, Ibaraki, Osaka 567-0085, Japan*
[c]*Graduate School of Pharmaceutical Sciences, Nagoya University, Furo-cho, Chikusa-ku, Nagoya, Aichi 464-8601, Japan*

†Electronic supplementary information (ESI) available: NMR spectra of new compounds, HPLC and MALDI-TOF MS analysis of modified ODNs, photoreaction of modified ODNs and UV melting curves for modified duplexes. See DOI: 10.1039/c3ob42427h

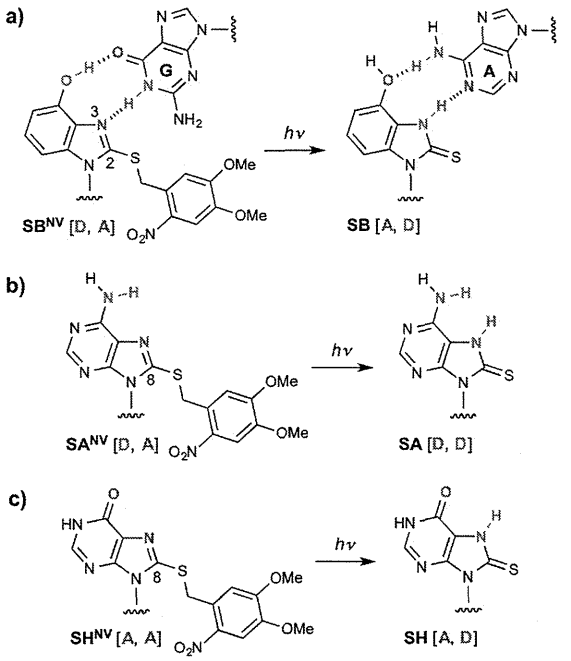

Fig. 1 (a) Change in base recognition by SB^{NV} upon photoirradiation. (b) Photoinduced changes in hydrogen bonding patterns of SA^{NV} and (c) SH^{NV}.

Fig. 1b and c). 8-Thiopurine analogues should preferentially adopt the *syn* conformation about the glycosidic bond due to steric repulsion between the C8-sulfur atom and the 4′-oxygen atom in the *anti* conformer.[16,17] SA^{NV} and SH^{NV} should also adopt the *syn* conformation and use the H-A and H-D Hoogsteen face to contact the target base. The H-bonding pattern of SA^{NV} and SH^{NV} at the Hoogsteen face would thus be changed from [D, A] to [D, D] and [A, A] to [A, D], respectively (Fig. 1). T_m evaluation of modified ODNs revealed that photoinduced changes in H-bonding patterns of 8-thiopurine nucleobase analogues have a pronounced effect on base recognition abilities.

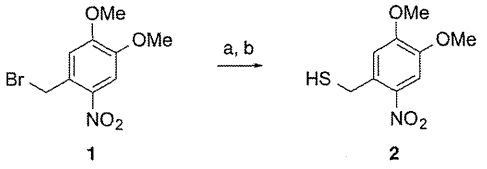

Scheme 1 Preparation of 6-nitroveratrylthiol **2**. *Reagents and conditions*: (a) KSAc, THF, rt; (b) conc. HCl aq., MeOH, 60 °C, 94% over two steps.

Results and discussion

The syntheses of the phosphoramidites bearing SA^{NV} and SH^{NV} as a nucleobase are summarized in Scheme 1. 6-Nitroveratrylthiol (**2**) was prepared from 6-nitroveratrylbromide (**1**) (Scheme 1) and subjected to reaction with 8-bromo-2′-deoxyadenosine derivative (**3**)[18] to afford **4** (Scheme 2). Phosphitylation at the 3′-hydroxyl group provided SA^{NV}-phosphoramidite **5**. For the preparation of SH^{NV}-phosphoramidite **9**, 8-bromoinosine (**6**)[19] was treated with **2** to give **7** (Scheme 3). Tritylation of the primary hydroxyl group in **7** and phosphitylation of the secondary hydroxyl group provided phosphoramidite **9**. Amidite blocks **5** and **9** were applied to an automated DNA synthesizer to incorporate SA^{NV} and SH^{NV} into ODNs. SA^{NV} and SH^{NV} were incorporated into the middle of the pyrimidine

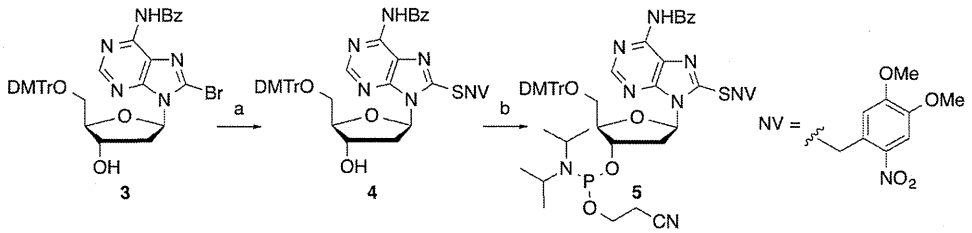

Scheme 2 Preparation of the phosphoramidites bearing SA^{NV}. *Reagents and conditions*: (a) **2**, K_2CO_3, DMF, rt, 52%; (b) $(iPr_2N)P(Cl)O(CH_2)_2CN$, iPr_2NEt, MeCN, rt, 77%.

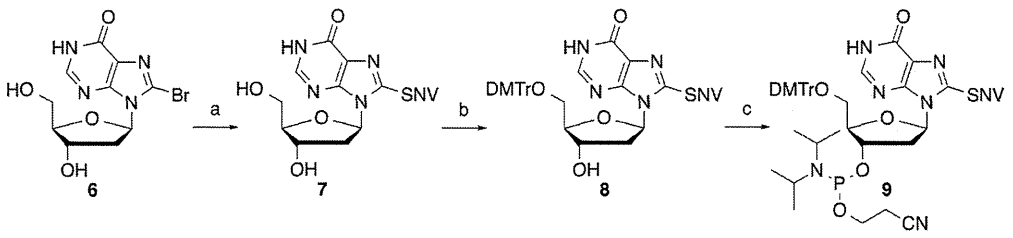

Scheme 3 Preparation of the phosphoramidites bearing SH^{NV}. *Reagents and conditions*: (a) **2**, K_2CO_3, DMF, rt, 25%; (b) DMTrCl, pyridine, rt, 85%; (c) $(iPr_2N)P(Cl)O(CH_2)_2CN$, iPr_2NEt, MeCN, rt, 74%.

10 5'-d(TCGTTT**SA**^{NV}TTGCG)-3'
11 5'-d(TCGTTT**SH**^{NV}TTGCG)-3'
12 5'-d(TCGTTTA TTGCG)-3'
13 5'-d(TCGTTTG TTGCG)-3'
14 3'-d(AGCAAAA AACGC)-5'
15 3'-d(AGCAAAG AACGC)-5'
16 3'-d(AGCAAAC AACGC)-5'
17 3'-d(AGCAAAT AACGC)-5'

Fig. 2 ODN sequences used in this study.

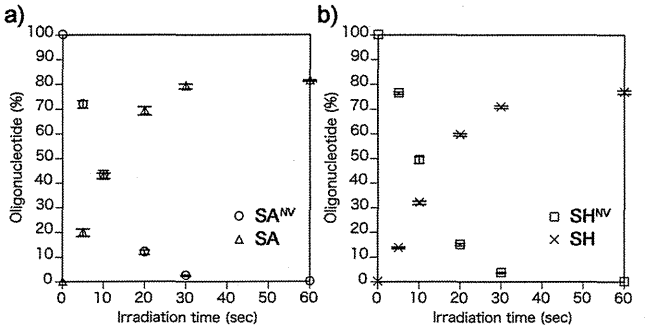

Fig. 3 Time course conversion of (a) SA^{NV} to SA in ODN **10** and (b) SH^{NV} to SH in ODN **11** by photoirradiation. Conditions: each ODN (0.1 nmol, 10 μM), sodium phosphate buffer (pH 7.2, 25 mM). Irradiation (365 nm) was performed at rt. Error bars indicate standard deviation (n = 3).

(T) strand of ODN **10** and ODN **11**. After cleavage from the resin and purification by reversed-phase (RP) HPLC, the structure of each ODN was confirmed by MALDI-TOF MS analysis. The sequence of each ODN used in this study is shown in Fig. 2.

The photoreactivity of **SA**^{NV} and **SH**^{NV} in a DNA strand was investigated by RP-HPLC analysis using ODN **10** and ODN **11**. When irradiated at 365 nm at 37 °C, ODN **10** and ODN **11** gradually disappeared. MALDI-TOF MS showed that the resulting ODNs were **SA**-/**SH**-ODNs and confirmed that the NV group of **SA**^{NV} and **SH**^{NV} was efficiently removed. Fig. 3 shows the percentage of the remaining **SA**^{NV}-/**SH**^{NV}- and resulting **SA**-/**SH**-ODNs at several irradiation time points. The photoreaction was complete within 60 s for both ODNs, and the yield of NV-removed ODNs was estimated from the HPLC peak area to be about 80%.

The effects of photoinduced changes in H-bonding patterns of **SA**^{NV} and **SH**^{NV} on their base recognition ability were examined by measuring the T_m values of DNA duplexes containing ODN **10** and ODN **11** (Table 1). ODN **10** and ODN **11** were individually hybridized to four ODNs, generating eight distinct duplexes in which each nucleobase analogue was paired with all possible natural nucleobases. For comparison, naturally matched duplexes containing the A : T and G : C base pairs in the same position were also examined. The duplex containing the **SA**^{NV} : G pair showed the highest T_m value of all the combinations of **SA**^{NV} with other nucleobases ($\Delta T_m \geqq 3$ °C). The

Table 1 T_m values of DNA duplexes[a]

5'-d(GCGTT**X**TTTGCT)-3'
3'-d(CGCAA**Y**AAACGA)-5'

Duplex	X : Y	T_m (°C) UV (−)	T_m [b] (°C) UV (+)
10 : 14	**SA**^{NV} : A	26	24
10 : 15	**SA**^{NV} : G	35	28
10 : 16	**SA**^{NV} : C	24	26
10 : 17	**SA**^{NV} : T	32	32
11 : 14	**SH**^{NV} : A	31	39
11 : 15	**SH**^{NV} : G	35	26
11 : 16	**SH**^{NV} : C	30	31
11 : 17	**SH**^{NV} : T	26	28
12 : 17	A : T	41	41
13 : 16	G : C	43	43
12 : 15	A : G (mismatch)	33	33
12 : 16	A : C (mismatch)	29	29
13 : 14	G : A (mismatch)	32	32
13 : 17	G : T (wobble)	35	35

[a] Conditions: each ODN (4.0 μM), NaCl (20 mM), sodium phosphate buffer (10 mM, pH 7.2). [b] T_m values of DNA duplexes after irradiation (365 nm) at 37 °C for 5 min.

SA^{NV} : G pair was slightly less stable than natural base pairs, and its stability was similar to the stability of the G : T wobble base pair. After photoirradiation at 365 nm for 5 min, **SA** showed the highest affinity towards thymine ($\Delta T_m \geqq 4$ °C); however, the T_m values of duplexes containing **SA** are, on the whole, low ($T_m \leqq 32$ °C). **SH**^{NV} in ODN **11** showed the highest affinity towards guanine, similar to **SA**^{NV} ($\Delta T_m \geqq 4$ °C). The T_m value of the duplex containing the **SH**^{NV} : G base pair was also slightly lower than that of natural duplexes. In contrast, after irradiation, the preferred base-pairing partner for **SH**^{NV} clearly changed to adenine ($\Delta T_m \geqq 8$ °C). Notably, the stability of **SH** : A was comparable to that of the natural A : T base pair. These results suggest that photoirradiation induces a change in base recognition by **SH**^{NV} from guanine to adenine. Fig. 4 illustrates the changes in the UV melting profiles of ODN-**11**-formed DNA duplexes and clearly indicates that the change in base recognition by **SH**^{NV} is triggered by photoirradiation.

Although further conclusive experiments such as NMR or X-ray structural analysis are needed to elucidate the precise base pair structures, the results of the T_m measurements suggest that **SA**^{NV} and **SH**^{NV} recognize guanine *via* two H bonds on the Hoogsteen face, as shown in Fig. 5. The stabilities of the **SA**^{NV} and **SH**^{NV} : G base pairs were slightly lower than that of the natural base pairs. It would appear that steric repulsion between the 8-sulfur atom in **SA**^{NV} and the 2-amino group in guanine decreases the stability of the **SA**^{NV} : G pair (Fig. 5a). This observation is consistent with previous reports showing that the base pair between 2-thiouracil and 2,6-diaminopurine is significantly destabilized because of steric hindrance.[20,21] Also, **SH**^{NV} may form a wobble pair with guanine similar to the U : G mismatch pair commonly found in RNA[22] (Fig. 5b); therefore, the **SH**^{NV} : G pair is less stable than natural base pairs. Light-induced changes in H-bonding patterns have profound effects on the base recognition abilities of 8-